Spectroscopic Studies of Oxidized Manganese Catalase and μ-Oxo-Bridged Dimanganese(III) Model Complexes: Electronic Structure of the Active Site and Its Relation to Catalysis

Thomas C. Brunold,[†] **Daniel R. Gamelin,**[†,‡] **Timothy L. Stemmler,**[§] **Sanjay K. Mandal,**[⊥]
William H. Armstrong,[⊥] **James E. Penner-Hahn,**[§] **and Edward I. Solomon*,**[†]

*Contribution from the Departments of Chemistry, Stanford University, Stanford, California 94305,
The University of Michigan, Ann Arbor, Michigan 48109, and Boston College,
Chestnut Hill, Massachusetts 02167*

Abstract: Spectroscopic and electronic structure studies of oxidized manganese catalase (OxMnCAT) and μ-oxo-di-μ-carboxylato-bridged dimanganese(III) model complexes are presented and discussed, providing, for the first time, a detailed experimental description of the catalytically relevant Mn(III)/Mn(III) binuclear active site of MnCAT. The absorption and MCD spectra of the synthetic complexes are similar to one another, indicating that the transitions below 30 000 cm^{-1} are inherent to the $[Mn^{III}_2O(OAc)_2]^{2+}$ core. A combination of Raman excitation profile and polarized single-crystal absorption measurements on $[Mn_2O(OAc)_2(Me_3tacn)_2]$-$(ClO_4)_2·H_2O$ and density functional electronic structure calculations are used to identify the key spectral features of the model complexes and their relation to the dominant Mn−O(oxo) bonding interaction in these dimers. On the basis of these results, analysis of the spectroscopic data of OxMnCAT leads to the proposal that the active site consists of two ferromagnetically coupled five-coordinate Mn(III) ions linked by a hydroxo bridge, contrasting previous proposals of an oxo bridge at this site. The interaction of OxMnCAT with azide, an electronic structural mimic of H_2O_2, has been studied using absorption and MCD spectroscopies. It appears that azide binds to both Mn(III) ions of the active site by displacement of one ligand on each metal, indicating that both ions are available for reaction with H_2O_2. The significance of our results with respect to the catalytic peroxide disproportionation reaction accomplished by MnCAT is discussed.

Introduction

There has been considerable interest in a related class of non-heme Fe and Mn metalloproteins that are known or thought to have carboxylate-bridged binuclear active sites. The diversity of the reactions carried out by this class of proteins[1−5] appears to parallel that observed for hemoproteins.[6] Reversible dioxygen binding to the diferrous active site of hemerythrin, a dioxygen carrier protein in invertebrates,[7] may be contrasted with the dioxygen activation by the diferrous sites of methane monooxygenase,[4] ribonucleotide reductase of *E. coli*,[8] and fatty acid desaturases.[9] Binuclear manganese sites are catalytically active in several metalloproteins including manganese catalase (MnCAT),[10−12] arginase,[13] and possibly manganese ribonucleotide reductase of *Corynebacterium ammoniagenes*.[14]

Catalases catalyze the disproportionation of hydrogen peroxide to dioxygen and water, protecting cells against oxidative damage. Although most catalases contain the iron−protoporphyrin IX prosthetic group, Mn catalases have been isolated from three bacteria, *Lactobacillus plantarum*,[10] *Thermus thermophilus*,[11] and *Thermoleophilum album*.[12] Crystal structures at 3.0 Å resolution of *L. plantarum*[15] and *T. thermophilus*[16] catalases show that the enzymes exist as hexamers of subunits, each containing a binuclear active site with a Mn···Mn separation of ∼3.6 Å, and that the overall protein folds are similar to that of hemerythrin (with four antiparallel α-helices). While both EPR[17] and EXAFS[18] data for the reduced Mn(II)/

[†] Stanford University.

[‡] Present address: The University of Bern, Freiestrasse 3, CH-3000 Bern 9, Switzerland.

[§] The University of Michigan.

[⊥] Boston College.

(1) Wieghardt, K. *Angew. Chem., Int. Ed. Engl.* **1989**, *28*, 1153.

(2) Feig, A. L.; Lippard, S. J. *Chem. Rev.* **1994**, *94*, 759.

(3) Holm, R. H.; Kennepohl, P.; Solomon, E. I. *Chem. Rev.* **1996**, *96*, 2239.

(4) Wallar, B. J.; Lipscomb, J. D. *Chem. Rev.* **1996**, *96*, 2625.

(5) Dismukes, G. C. *Chem. Rev.* **1996**, *96*, 2909.

(6) Babcock, G. T.; Floris, R.; Nilsson, T.; Pressler, M.; Varotsis, C.; Vollenbrock, E. *Inorg. Chim. Acta* **1996**, *243*, 345.

(7) Stenkamp, R. E. *Chem. Rev.* **1994**, *94*, 715.

(8) Logan, D. T.; Su, X.-D.; Åberg, A.; Regnström, K.; Hajdu, J.; Eklund, H.; Nordlund, P. *Struct. Bonding (Berlin)* **1996**, *4*, 1053.

(9) Lindqvist, Y.; Huang, W.; Schneider, G.; Shanklin, J. *EMBO J.* **1996**, *15*, 4081.

(10) (a) Kono, Y.; Fridovich, I. *J. Biol. Chem.* **1983**, *258*, 6015. (b) Beyer, W. F. J.; Fridovich, I. *Biochemistry* **1985**, *24*, 6460.

(11) Barynin, V. V.; Grebenko, A. I. *Dokl. Akad. Nauk. SSSR* **1986**, *286*, 461.

(12) Algood, G. S.; Perry, J. J. *J. Bacteriol.* **1986**, *168*, 563.

(13) (a) Hertzfeld, A.; Raper, S. M. *J. Biochem.* **1976**, *153*, 469. (b) Kanyo, Z. F.; Scolnick, L. R.; Ash, D. E.; Christianson, D. W. *Nature* **1996**, *383*, 554.

(14) (a) Auling, G.; Follmann, H. In *Metal ions in biological systems*; Sigel, H., Sigel, A., Eds.; Dekker: New York, 1994; pp 132−161. (b) Griepenburg, U.; Lassmann, G.; Auling, G. *Free Radical Res.* **1996**, *26*, 473.

(15) Baldwin, E. Thesis, University of North Carolina, Chapel Hill, 1990.

(16) Vanishtein, B. K.; Melik-Adamyan, W. R.; Barynin, V. V.; Vagin, A. A. In *Progress in Bioinorganic Chemistry and Molecular Biology;* Ovchinnikov, Y., Ed.; Elsevier: Amsterdam, 1984; pp 117−132.

(17) Khangulov, S. V.; Pessiki, P. J.; Barynin, V. V.; Ash, D. E.; Dismukes, G. C. *Biochemistry* **1995**, *34*, 2015.

Mn(II) enzymes are consistent with a Mn···Mn separation of 3.5−3.6 Å, a preliminary report of the high-resolution crystal structures for the Mn(II)/Mn(II) and Mn(III)/Mn(III) forms of *T. thermophilus* catalase gives Mn···Mn distances of 3.18 and 3.14 Å, respectively.[19] A refined atomic map of the *L. plantarum* enzyme is nearing completion (V. Barynin, private communication).

Mn catalases can be prepared in a variety of oxidation states, ranging from the reduced Mn(II)/Mn(II) to the superoxidized Mn(III)/Mn(IV) forms.[20,21] Activity measurements and numerous spectroscopic studies of the reduced Mn(II)/Mn(II) and mixed valence Mn(II)/Mn(III) and Mn(III)/Mn(IV) derivatives have provided some insight into the catalytic mechanism of Mn catalases.[5] Of the several oxidation states observed, only the Mn(II)/Mn(II) and Mn(III)/Mn(III) oxidation states are believed to participate in the catalytic cycle.[22] The ratio of the reduced and oxidized forms of *L. plantarum* catalase is ∼2/1 both under turnover conditions and following incubation with dioxygen.[22] A variety of anions, including N_3^-, F^-, and Cl^-, have been shown to inhibit Mn catalase, although only at concentrations that are orders of magnitude higher than those required to inhibit heme catalases.[20,21,23,24] Azide and halide inhibitors strongly affect the EPR signal of the Mn(II)/Mn(II) catalase and alter the exchange coupling between the two Mn(II) atoms. If peroxide is added in the presence of halide inhibitors, the enzyme is trapped in the reduced state.[22]

The reduced form has been studied extensively using EPR and EXAFS spectroscopies, from which it has been proposed to contain a binuclear Mn(II)/Mn(II) active site with mixed O and N ligation and a water-derived bridging ligand[17,18] (μ-aqua or μ-hydroxo). By contrast, the lack of an EPR signal[20] and the facile X-ray photoreduction[22] of oxidized MnCAT (OxMn-CAT) have made characterization of this form inaccessible. The similar overall protein folds of MnCAT and hemerythrin and the resemblance of the absorption spectra of OxMnCAT and synthetic μ-oxo-di-μ-carboxylato-bridged manganese(III) dimers have led to the idea that a $[Mn^{III}_2O(O_2CR)_2]^{2+}$ core may be present in the oxidized enzyme.[1,5,25] Similar absorption spectra are also observed for monomeric Mn(III) complexes,[26−29] however, and further characterization of the geometric and electronic structures of the oxidized active site is required to obtain significant insight into the reaction mechanism of MnCAT.

(18) Stemmler, T. L.; Sossong, T. M.; Goldstein, J. I.; Ash, D. E.; Elgren, T. E.; Kurtz, D. M., Jr.; Penner-Hahn, J. E. *Biochemistry* **1997**, *36*, 9847.

(19) Barynin, V. V.; Hempstead, P. D.; Vagin, A. A.; Antonyuk, S. V.; Melik-Adamyan, W. R.; Lamzin, V. S.; Harrison, P. M.; Artymiuk, P. J. *J. Inorg. Biochem.* **1997**, *67*, 196.

(20) Khangulov, S. V.; Barynin, V. V.; Voevodskaya, N. V.; Grebenko, A. I. *Biochim. Biophys. Acta* **1990**, *1020*, 305.

(21) Penner-Hahn, J. E. In *Manganese Redox Enzymes;* Pecoraro, V. L., Ed.; VCH Publishers: New York, 1992; pp 29−45.

(22) Waldo, G. S.; Penner-Hahn, J. E. *Biochemistry* **1995**, *34*, 1507.

(23) Khangulov, S. V.; Goldfeld, M. G.; Gerasimenko, V. V.; Andreeva, N. E.; Barynin, V. V.; Grebenko, A. I. *J. Inorg. Biochem.* **1990**, *40*, 279.

(24) Meier, A. E.; Whittaker, M. M.; Whittaker, J. W. *Biochemistry* **1996**, *35*, 348.

(25) Sheats, J. E.; Czernuszewicz, R. S.; Dismukes, G. C.; Rheingold, A. L.; Petrouleas, V.; Stubbe, J.; Armstrong, W. H.; Beer, R. H.; Lippard, S. J. *J. Am. Chem. Soc.* **1987**, *109*, 1435.

(26) (a) Dingle, R. *Inorg. Chem.* **1965**, *4*, 1287. (b) Dingle, R. *Acta Chem. Scand.* **1966**, *20*, 33. (c) Dingle, R. *J. Mol. Spectrosc.* **1962**, *9*, 426.

(27) (a) Davis, T. S.; Fackler, J. P.; Weeks, M. J. *Inorg. Chem.* **1968**, *7*, 1994. (b) Boucher, L. J.; Herrington, D. R. *Inorg. Chem.* **1974**, *13*, 1105. (c) Boucher, L. J.; Day, V. W. *Inorg. Chem.* **1977**, *16*, 1360. (d) Wieghardt, K.; Pohl, K.; Bossek, U.; Nuber, B.; Weiss, J. *Z. Naturforsch.* **1988**, *43b*, 1184.

(28) Lever, A. B. P. *Inorganic Electronic Spectroscopy*, 2nd ed.; Elsevier Science Publishers B. V.: Amsterdam, 1984.

(29) Whittaker, J. W.; Whittaker, M. M. *J. Am. Chem. Soc.* **1991**, *113*, 5528.

In the present study a combination of absorption, CD, and variable-temperature variable-field MCD spectroscopies are used to provide, for the first time, a detailed experimental description of the catalytically active Mn(III)/Mn(III) binuclear site of OxMnCAT and its interaction with azide, an electronic structural mimic of hydrogen peroxide. To facilitate the interpretation of these data, absorption, MCD, and resonance Raman experiments were performed on a series of synthetic complexes containing μ-oxo-di-μ-carboxylato-bridged dimanganese(III) units previously proposed to model the active site in OxMnCAT. In these complexes Mn(III) is stabilized in an axially compressed (along the Mn−(μ−O) bond) octahedral coordination. Polarized single-crystal absorption data obtained for $[Mn_2O(OAc)_2(Me_3tacn)_2](ClO_4)_2·H_2O$, complemented by density functional electronic structure calculations, are used to assign the key spectral features of the model complexes. On the basis of these results, density functional calculations are employed to correlate geometric perturbations with changes in electronic structure in order to evaluate key structural elements of the active site in OxMnCAT. The significance of our results with respect to the catalytic peroxide disproportionation accomplished by MnCAT is discussed.

Experimental Section

Mn catalase was isolated from *L. plantarum* according to established procedures.[10,30] Resting enzyme was prepared by fully reducing the as-isolated catalase by anaerobic incubation with hydroxylamine followed by incubation with hydrogen peroxide. The resting enzyme exists as a ∼60/40 mixture of the Mn(II)/Mn(II) and Mn(III)/Mn(III) forms with no detectable Mn(III)/Mn(IV) fraction.[22] Azide-perturbed protein was formed by addition of 100-fold excess NaN_3 to the resting enzyme. Absorption and MCD data were collected in 70/30 D-glycerol/D_2O 50 mM phosphate buffer glasses at pH 7.

Samples of $[Mn_2O(OAc)_2(Me_3tacn)_2](ClO_4)_2·H_2O$,[31] $[Mn_2O(OAc)_2\{HB(pz)_3\}_2]$,[25] $[Mn_2O(OAc)_2(bpea)_2](ClO_4)_2$,[32] and $[Mn_2O(OAc)_2(tppn)]_2(ClO_4)_4$ were prepared according to literature procedures. Absorption and MCD data were obtained on polycrystalline samples dispersed in poly(dimethylsiloxane) mulling agent. Single crystals of $[Mn_2O(OAc)_2(Me_3tacn)_2](ClO_4)_2·H_2O$ of appropriate thickness for polarized absorption measurements were grown on quartz disks at 4 °C from acetonitrile solution. This compound crystallizes in the orthorhombic space group *Amam* with four symmetry-related molecules per unit cell.[31] The dimeric units possess crystallographically imposed C_{2v} symmetry with all Mn···Mn vectors aligned parallel to **c**, and each monomer half has C_s symmetry with a mirror plane σ ⊥ **a**. These crystals exhibit a marked dichroism: They are deep red for linearly polarized light with **E** ⊥ **a** and colorless for **E** ∥ **a**.

Low-temperature absorption spectra were measured on a double-beam spectrophotometer (Cary 17) using a liquid helium cryostat (Janis Research Super Vari-Temp). A pair of Glan-Taylor polarizers matched from 200 nm to 2.5 μm were used for single-crystal experiments. CD and MCD data were collected on CD spectropolarimeters (Jasco J200 and J500) with sample compartments modified to accommodate magnetocryostats (Oxford Instruments). Raman spectra were recorded for a series of lines of Kr^+ (Coherent I90C-K) and Ar^+ (Coherent Sabre 25/7) ion lasers with incident power in the 5−25 mW range using a ∼135° back-scattering arrangement. Solid samples were spun in sealed quartz capillary tubes and cooled to about 120 K using a nitrogen gas flow system. The scattered light was dispersed by a triple monochromator (Spex 1877 CP, equipped with 1200, 1800, and 2400 grooves/mm gratings) and detected with a back-illuminated CCD camera (Princeton Instruments ST-135). Raman intensities were calibrated relative to the 984 cm^{-1} scattering peak of K_2SO_4.

(30) Stemmler, T. L. Ph.D. Thesis, The University of Michigan, 1996.

(31) Wieghardt, K.; Bossek, U.; Ventur, D.; Weiss, J. *J. Chem. Soc., Chem. Commun.* **1985**, 347.

(32) Mandal, S. K.; Armstrong, W. H. *Inorg. Chim. Acta* **1995**, *229*, 261.
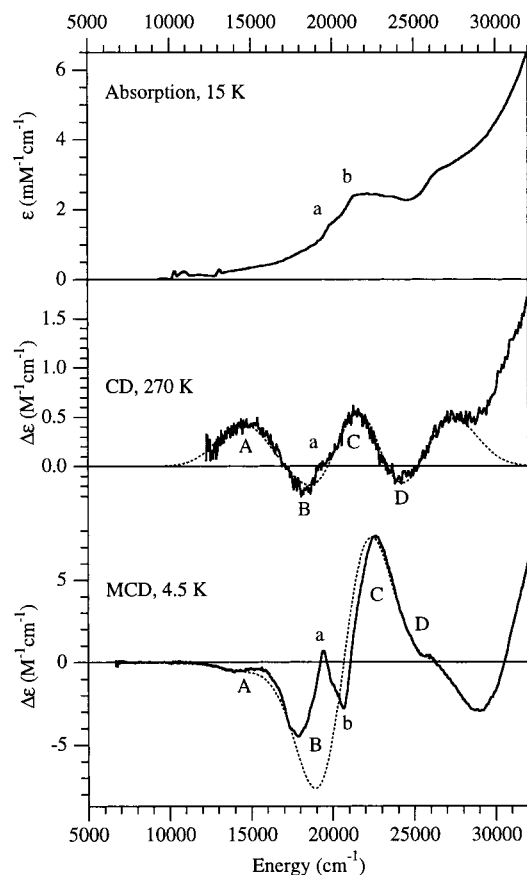
Figure 1. 15 K absorption, 270 K CD, and 4.5 K MCD (5.5 T) spectra of resting Mn catalase in ~70% D-glycerol glass (solid lines). ϵ values are given per Mn(III)/Mn(III) dimer of the oxidized component (OxMnCAT). Gaussian fits of the CD and MCD spectra are shown by the broken lines (see Table 1 for band assignments and fit parameters).

Ligand field calculations within the framework of the angular overlap model were carried out employing the Ligfield computer program developed by Bendix.[33] Density functional calculations were performed on an IBM 3BT-RS/6000 computer using the Amsterdam Density Functional (ADF) program version 2.0.1 developed by Baerends et al.[34] A triple-ζ Slater-type orbital basis set (ADF basis set IV) with a single polarization function was used for each atom. Core orbitals were frozen through 1s (C, N, O) and 3p (Mn). All calculations were performed single point using the local density approximation of Vosko, Wilk, and Nusair[35] for the exchange and correlation energy and the nonlocal gradient corrections of Becke[36] and Perdew.[37] The accuracy parameter for the numerical integration grid used was 4.0. Complete coordinates of all the models discussed in the text are included in the Supporting Information (Tables S1–S4). Graphical output of the computational results was generated with the Cerius[2] software program developed by Molecular Simulations Inc.

Results and Analysis

(1) Excited States. Manganese Catalase. The low-temperature absorption and MCD spectra and 270 K CD spectrum of resting Mn catalase (MnCAT) are shown in Figure 1. Since all Mn(II) d → d transitions are spin forbidden, the dominant features in the visible and near-IR regions can be attributed to the oxidized component. This was verified by measuring the

(33) Bendix, J. *Ligfield version 0.85*; (Department of Chemistry, University of Copenhagen, Universitetsparken 5, DK 2100, Denmark.
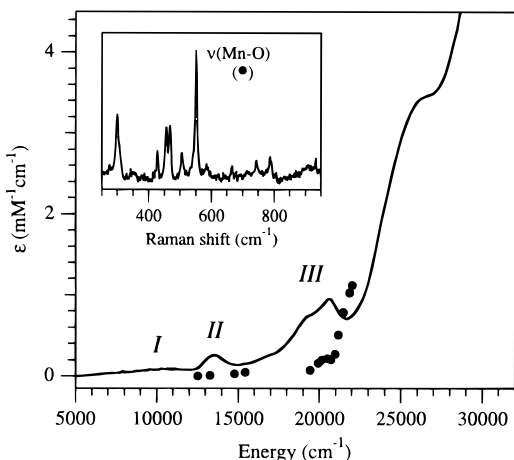(34) (a) Baerends, E. J.; Ellis, D. E.; Ros, P. *Chem. Phys.* **1973**, *2*, 42. (b) te Velde, G.; Baerends, E. J. *Int. J. Comput. Phys.* **1992**, *99*, 84.
(35) Vosko, S. H.; Wilk, L.; Nusair, M. *Can. J. Phys.* **1980**, *58*, 1200.
(36) Becke, A. D. *J. Chem. Phys.* **1986**, *84*, 4524.
(37) Perdew, J. P. *Phys. Rev. B* **1986**, *33*, 8822.

Table 1. Fit Parameters from Simultaneous Gaussian Resolutions of the Absorption, CD, and MCD Spectra of OxMnCAT in Figure 1[a]

band	$^5A(z^2) \rightarrow$	ν_{max}	$\nu_{1/2}$	ϵ	$\Delta\epsilon_{CD}$	$\Delta\epsilon_{MCD}$	azide shift[b]
A	$^5A(x^2\text{-}y^2)$	14 500	3050	250	0.4	−0.5	−1700
B	$^5A(xy)$	19 400	3050	800	−0.4	−9.5	−900
C	$^5A(xz)$	22 000	3050	1350	1.2	10.3	−750
D	$^5A(yz)$	23 200	3050	1250	−0.8	−1.0	−100
a[c]	$^3\Gamma$ [^{3}H]	19 380	~1000				−100
b[c]	$^3\Gamma\,'$ [^{3}H]	20 670	~1000				0

[a] Band maxima ν_{max} and bandwidths at half-maximum $\nu_{1/2}$ are in cm^{-1} and molar extinction coefficients ϵ and ellipticities $\Delta\epsilon$ in M^{-1} cm^{-1}. Band assignments are given in monomer notation (C_1 symmetry) and relate to Figure 10. [b] Estimated band shifts (cm^{-1}) occurring upon azide binding to OxMnCAT (from Gaussian fit of MCD spectrum, Figure S4). [c] From MCD spectrum.

absorption and MCD spectra of a sample containing ~95% reduced MnCAT. No new features were observed but only reduced intensity of the oxidized MnCAT (OxMnCAT) signal.

In the 15 K absorption spectrum, a broad band centered at about 21 000 cm^{-1} ($\epsilon \approx 2500$ M^{-1} cm^{-1} [38]) and exhibiting two poorly resolved shoulders on its low-energy side is the dominant feature in the visible and near-IR regions (the group of sharp lines below 14 000 cm^{-1} arise from vibrational overtones of the protein). This band is characteristic of Mn(III); in monomers it is typically observed at ~20 000 cm^{-1} ($\epsilon \approx 50$ M^{-1} cm^{-1} in six-coordinate octahedral and ~800 M^{-1} cm^{-1} in five-coordinate complexes) and assigned to the 10 Dq ligand-field transition.[26–28] Above 25 000 cm^{-1} a weak shoulder located at ~26 500 cm^{-1} is the only discernible feature on the rising background. Varying the temperature between 15 and 300 K has practically no effect on the absorption spectrum, indicating that the active site geometry of OxMnCAT is preserved upon cooling.

More features are resolved in the CD and MCD spectra. The 270 K CD spectrum of OxMnCAT (Figure 1, middle) exhibits a series of four broad bands (labeled A–D) below 25 000 cm^{-1}. The intensity increases into the UV with a positive maximum above 32 000 cm^{-1} and a positive shoulder at ~27 500 cm^{-1}. Bands A–D are also observed in the 4.5 K MCD spectrum (Figure 1, bottom), with bands A and D being very weak. The highest MCD intensity in the visible and near-IR regions involves bands B and C, which give rise to a pair of MCD bands of opposite signs but similar intensities. The high-energy side of band B is greatly distorted by the presence of two oppositely signed sharp features (a and b) which can be related to the two shoulders in the absorption spectrum.

The CD and MCD spectra below 25 000 cm^{-1} are simultaneously well fit with a set of four Gaussians[39] corresponding to bands A–D (dotted lines). While the Gaussian fit of the absorption spectrum (not shown) is susceptible to baseline uncertainties, a rough estimate of band intensities can be obtained. The fit parameters are summarized in Table 1.

μ-Oxo-Bridged Dimanganese(III) Model Complexes. The 5 K solid-state mull absorption spectrum of [Mn$_2$O(OAc)$_2$(Me$_3$-tacn)$_2$](ClO$_4$)$_2 \cdot$H$_2$O is shown in Figure 2. Similar to OxMnCAT (Figure 1), the dominant feature in the visible and near-IR regions consists of a broad band (designated *III*) centered at ~20 500 cm^{-1} ($\epsilon = 900$ M^{-1} cm^{-1}) with two shoulders at 19 600 and 20 600 cm^{-1}. In contrast to the protein spectrum, however, it exhibits an additional rather intense band (*II*) peaking at 13 500 cm^{-1} ($\epsilon = 250$ M^{-1} cm^{-1}) and a weak broad feature (*I*) centered at ~10 000 cm^{-1} ($\epsilon \approx 60$ M^{-1} cm^{-1}). In

(38) ϵ and $\Delta\epsilon$ are given per Mn(III)/Mn(III) dimer of OxMnCAT.
(39) A fifth band was used in the Gaussian fit of the CD spectrum to simulate the positive shoulder at 27 500 cm^{-1}.

Figure 2. Solid-state 5 K mull absorption spectrum and ∼120 K resonance Raman excitation profile for the symmetric Mn−O stretching mode ν(Mn−O) (●) of $[Mn_2O(OAc)_2(Me_3tacn)_2](ClO_4)_2\cdot H_2O$. Inset: Resonance Raman spectrum obtained with 455 nm (21 980 cm^{-1}) excitation. The ν(Mn−O) fundamental band is indicated.

Figure 3. $\mathbf{E} \parallel \mathbf{a}$ (dotted line) and $\mathbf{E} \perp \mathbf{a}$ (solid line) polarized single-crystal absorption spectra of $[Mn_2O(OAc)_2(Me_3tacn)_2](ClO_4)_2\cdot H_2O$ at 5 K.

the UV the onset to a very strong absorption is observed with a maximum above 30 000 cm^{-1} and a shoulder at 26 000 cm^{-1}.

The most intense feature in the ∼120 K resonance Raman spectrum of solid $[Mn_2O(OAc)_2(Me_3tacn)_2](ClO_4)_2\cdot H_2O$ obtained with 455 nm (21 980 cm^{-1}) excitation consists of a sharp peak at 552 cm^{-1} (inset of Figure 2), assigned to the symmetric Mn−O stretching mode ν(Mn−O) as this is typically observed in this region.[25] The corresponding resonance Raman excitation profile is superimposed on the absorption spectrum in Figure 2. It shows practically no enhancement below 21 000 cm^{-1} but strongly increases into the UV.

The 5 K $\mathbf{E} \parallel \mathbf{a}$ and $\mathbf{E} \perp \mathbf{a}$ polarized single-crystal absorption spectra of $[Mn_2O(OAc)_2(Me_3tacn)_2](ClO_4)_2\cdot H_2O$ in the visible and near-IR regions are shown in Figure 3. The two polarizations are remarkably different; while band *II* is $\mathbf{E} \parallel \mathbf{a}$ polarized, i.e., perpendicular to the Mn−O−Mn plane, the stronger feature centered at 20 500 cm^{-1} (band *III*) is exclusively observed in $\mathbf{E} \perp \mathbf{a}$ polarization.[40]

A comparison of the low-temperature MCD spectra of a series of four μ-oxo-di-μ-carboxylato-bridged Mn(III) dimers and

_____

(40) Note that the ∼20 500 cm^{-1} band appears to be much sharper than in solution spectra recorded at room temperature. This is due to strong antiferromagnetic exchange interactions in the corresponding excited state and will be discussed elsewhere. Brunold, T. C.; Gamelin, D. R.; Solomon, E. I. Manuscript in preparation.
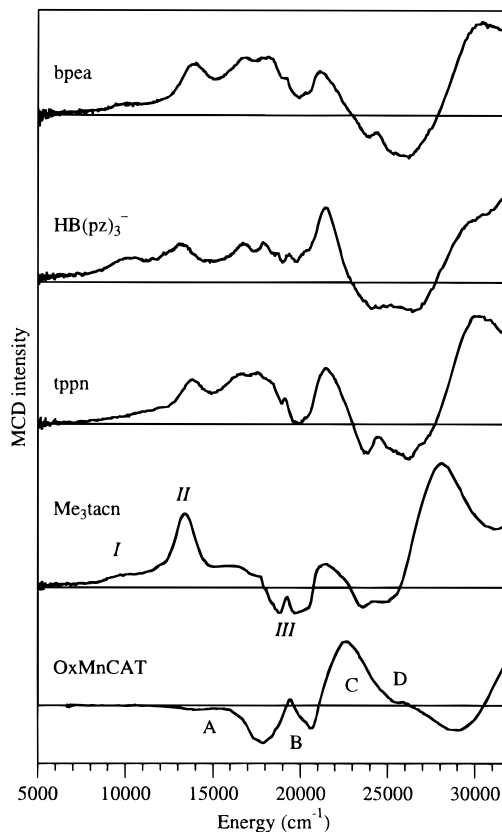

Figure 4. 4.5 K MCD spectra of a series of four synthetic complexes containing μ-oxo-di-μ-carboxylato-bridged Mn(III) dimers (labeled according to the capping ligands) and OxMnCAT.

OxMnCAT is given in Figure 4. While the spectra of the synthetic complexes are similar to one another, indicating that the transitions below ∼30 000 cm^{-1} are inherent to the $[Mn^{III}_2O(OAc)_2]^{2+}$ core, they show a number of striking differences from the protein spectrum: A large imbalance between positive and negative intensity, the presence of a broad feature (*I*) with a maximum around 10 000 cm^{-1} and tailing to ∼5000 cm^{-1}, and an intense positive band (*II*) at ∼13 500 cm^{-1} (notice that bands *I* and *II* are also observed in absorption; cf. Figures 2 and 3). In contrast, an MCD spectrum very similar to that of OxMnCAT has been reported for Mn(III) superoxide dismutase (MnSOD),[29] a mononuclear enzyme with a five-coordinate, trigonal bipyramidal active site (vide infra). A comparison of the two spectra is provided as Supporting Information (Figure S1).

Spectral Assignments for the Model Complexes. Band assignments for the spectra of OxMnCAT (Figure 1) are complicated by the fact that details of the active site structure are not yet known.[19] It is thus of significant interest to understand the above-mentioned differences in the spectroscopy of OxMnCAT and the synthetic $[Mn^{III}_2O(OAc)_2L_2]^{2+}$ model complexes. In this section the polarized single-crystal absorption data (Figure 3) are complemented by density functional calculations to unambiguously assign bands *I−III*. Together with the results from the ground-state analysis (next section) this will establish the necessary background for analysis of the OxMnCAT spectroscopy (section 3).

The lack of resonance Raman enhancement of ν(Mn−O) below 21 000 cm^{-1} (Figure 2) demonstrates that bands *I−III* (and by analogy bands A−D in the spectra of OxMnCAT in Figure 1) are primarily d → d in character. Mn(III) has the 3d^4 electron configuration so that four of the five d orbitals will be half-occupied in a high-spin complex. A schematic
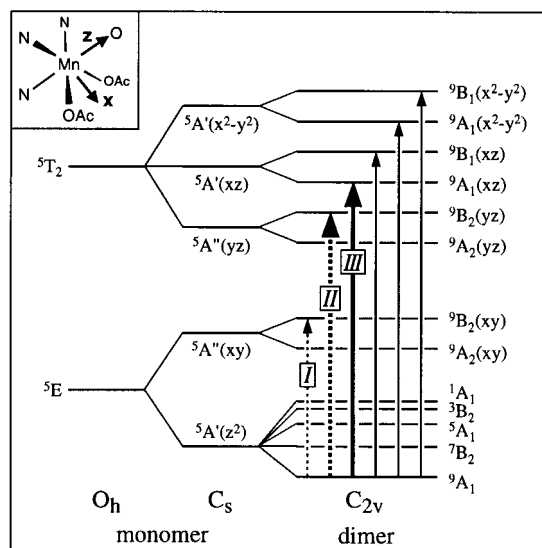
Figure 5. Schematic energy level diagram for the quintet ligand field states of Mn(III) in $[Mn_2O(OAc)_2(Me_3tacn)_2](ClO_4)_2 \cdot H_2O$ showing the effects of the $O_h \rightarrow C_s$ symmetry reduction and dimer formation (only the $S = 4$ components of the excited states are shown). Electric dipole allowed transitions and their polarizations in the C_{2v} dimer symmetry are sketched by arrows: **E** || **y(a)** (dotted lines) and **E** $\perp$ **y(a)** (solid lines). The two dominant transitions in absorption are highlighted by thick arrows (cf. Figure 3).

Chart 1. μ-O Me$_3$tacn Model and Coordinate Frames Used for the Electronic Structure Calculations
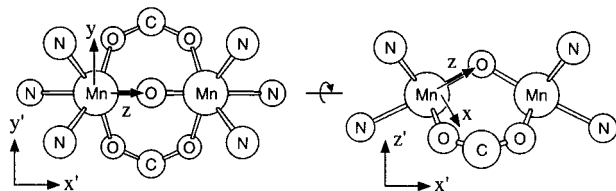
energy level diagram of the quintet ligand field (LF) states of Mn(III) in $[Mn_2O(OAc)_2(Me_3tacn)_2](ClO_4)_2 \cdot H_2O$ is shown in Figure 5 (see Chart 1 for axes orientations[41]). The strong axial LF component associated with the μ-oxo bridge lifts the degeneracies of the d orbitals and produces a hole in the z^2 orbital, which is oriented toward this bridge (throughout this study an abbreviated notation is used for d orbitals, e.g., z^2 standing for d_{z^2}). This gives rise to a total of four quintet LF excited states above the $^5A'(z^2)$ ground state in the C_s monomer symmetry (states are labeled as hole states).

Upon formation of the dimer the ground state splits into five components due to exchange interactions between the two $S = 2$ monomers, giving rise to the spin ladder shown in the right bottom portion of Figure 5. The LF excited states in the dimer are obtained by coupling the $^5A'(z^2)$ ground state of one Mn-(III) with the quintet excited state of its partner.[42] Since either one of the two metal ions can be excited, each singly excited configuration in the dimer is 2-fold degenerate. The proper dimer wave functions are given by the symmetric and antisymmetric combinations of the locally excited configurations, and the corresponding states are split by Coulomb and exchange-mediated excitation transfer interactions between the metal

centers[43,44] (Figure 5, right-hand side). Magnetic susceptibility measurements on $[Mn_2O(OAc)_2(Me_3tacn)_2](ClO_4)_2 \cdot H_2O$ have shown[45] that the two Mn(III) ions are weakly ferromagnetically coupled in the ground state, $J = +9$ cm^{-1} ($\mathcal{H} = -2J\mathbf{S}_1 \cdot \mathbf{S}_2$). Thus, at low temperatures only transitions originating from the $^9A_1$ component of the exchange-split ground state contribute to the absorption intensity. Their polarizations in C_{2v} symmetry are given by arrows in Figure 5: dotted and solid lines correspond to **E** || **y(a)** and **E** $\perp$ **y(a)** polarized transitions, respectively.

From Figure 5, only two transitions are expected in **E** || **y(a)** polarization. $^9A_1 \rightarrow {}^9B_2(xy)$ involves excitation of an electron within the split e_g set of d orbitals. For six-coordinate complexes this transition is usually observed between 5000 and 12 000 cm^{-1} [26-28] and the lowest-energy absorption and MCD band *I* in Figures 2 and 4 is therefore assigned to $^9A_1 \rightarrow {}^9B_2(xy)$. This is supported by the fact that for di-μ-oxo-bridged Mn(III)/Mn-(IV) dimers, where two oxo ligands contribute to the splitting of the e_g orbitals, the corresponding transition is observed between 10 000 and 13 000 cm^{-1}.[46] Note that tailing of band *I* to $\sim$5000 cm^{-1} suggests that the $^9B_2(xy)$ excited state is sufficiently low in energy to spin–orbit couple to the ground state, giving rise to the imbalance between positive and negative intensity in the MCD spectrum. The prominent absorption band *II* at $\sim$13 500 cm^{-1} in Figure 2 is then assigned to the second, higher-energy **E** || **y(a)** polarized transition $^9A_1 \rightarrow {}^9B_2(yz)$.

To understand in more detail the origin of band *II*, which appears to be a key spectral feature of $[Mn^{III}_2O(OAc)_2L_2]^{2+}$ complexes, and to assign band *III*, both high-spin (HS) and broken symmetry (BS) density functional calculations were performed on a simplified model of $[Mn_2O(OAc)_2(Me_3tacn)_2]^{2+}$ in which formates replace the acetates and NH$_3$ ligands replace the Me$_3$tacn ligation.[47] Two different views of this $[Mn_2O(O_2-CH)_2(NH_3)_6]^{2+}$ model (denoted μ-O Me$_3$tacn in the following) together with the molecular (primed) and local (unprimed) coordinate frames are shown in Chart 1.[41] The HS or ferromagnetic state with $S = 4$, $|M_S| = 4$, is the only ground-state spin component of an exchange-coupled Mn(III) dimer that can be described by a single determinant. Energies and compositions of the Mn d-based spin-up orbitals obtained from a spin-unrestricted HS calculation on μ-O Me$_3$tacn are given in Table 2, and an energy level diagram is shown in Figure S2 (Supporting Information).[48] The 10 manganese d-based MOs arise from symmetric ($+$) and antisymmetric ($-$) combinations (with respect to the molecular C_2 axis) of the 5 monomeric d orbitals with equal single-site contributions and additional ligand contributions of the appropriate symmetry. In the ferromagnetic ground state the four d electrons of each Mn ion occupy 8 of the 10 spin-up orbitals, leaving holes in the z^2-based MOs (levels

(41) Compared to the commonly used axis system the **x** and **y** axes are here rotated around **z** by 45°, thus, the e_g set of Mn d orbitals is comprised of the z^2 and xy orbitals. In $[Mn_2O(OAc)_2(Me_3tacn)_2](ClO_4)_2 \cdot H_2O$ the molecular **x'**, **y'**, and **z'** axes coincide with the crystallographic **c**, **a**, and **b** axes, respectively.

(42) Hirst, L. L.; Ray, T. *Proc. R. Soc. London, A* **1982**, *384*, 191.

(43) Eickman, N. C.; Himmelwright, R. S.; Solomon, E. I. *Proc. Natl. Acad. Sci. U.S.A.* **1979**, *76*, 2094.

(44) Güdel, H. U.; Weihe, H. In *Molecular Magnetism: From Molecular Assemblies to the Devices;* Coronado, E., et al., Eds.; Kluwer Academic: Dordrecht, The Netherlands, 1996; pp 173−197.

(45) Wieghardt, K.; Bossek, U.; Nuber, B.; Weiss, J.; Bonvoisin, J.; Corbella, M.; Vitols, S. E.; Girerd, J.-J. *J. Am. Chem. Soc.* **1988**, *110*, 7398.

(46) Gamelin, D. R.; Kirk, M. L.; Stemmler, T. L.; Pal, S.; Armstrong, W. H.; Penner-Hahn, J. E.; Solomon, E. I. *J. Am. Chem. Soc.* **1994**, *116*, 2392.

(47) (a) Previous calculations in ref 47b have focused on calculating ground-state exchange coupling constants and charge and spin densities. (b) Zhao, X. G.; Richardson, W. H.; Chen, J.-L.; Li, L.; Noodleman, L.; Tsai, H.-L.; Hendrickson, D. N. *Inorg. Chem.* **1997**, *36*, 1198.

(48) A verification of the electronic structure calculations is found from a comparison of the calculated and experimental J values. Using the formalism developed by Noodleman (Noodleman, L. *J. Chem. Phys.* **1981**, *74*, 5737) and the total energies of the HS and BS states a value of $J = -5$ cm^{-1} was obtained, in good agreement with the experimental value[45] ($J = +9$ cm^{-1}).

Table 2. Energies (eV) and Compositions (%) of the Mn d-Based Spin-Up Molecular Orbitals Obtained from a HS Calculation on μ-O Me$_3$tacn[a]
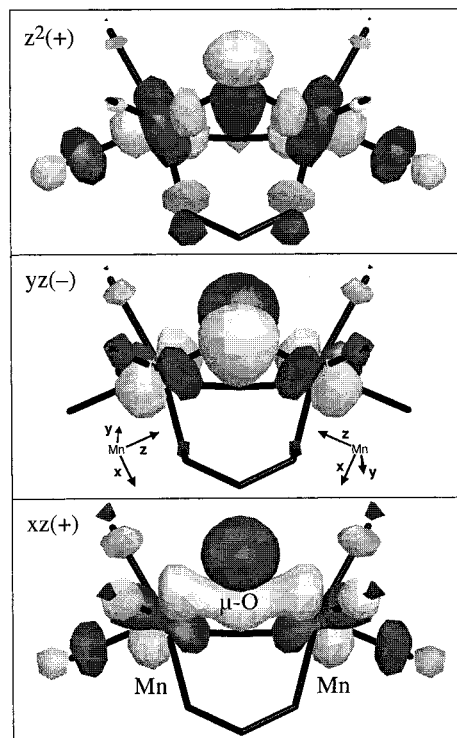
level	energy	Mn					μ-oxo			N,O′
		x^2-y^2	xz	yz	xy	z^2	$p_{x'}$	$p_{y'}$	$p_{z'}$	tot[b]
					unoccupied					
z^2 (−) 15b$_1$	−9.927	1	0	0	0	51	22	0	0	20
z^2 (+) 17a$_1$	−10.293	0	4	0	0	52	0	0	18	22
					occupied					
xy(−) 13b$_2$	−10.869	0	0	0	54	0	0	0	0	38
xy(+) 11a$_2$	−11.168	0	0	0	58	0	0	0	0	38
yz(−) 12b$_2$	−11.966	0	0	43	0	0	0	51	0	6
x^2-y^2 (−) 14b$_1$	−12.719	58	0	0	0	0	0	0	0	40
xz(+) 16a$_1$	−12.805	1	42	0	0	9	0	0	31	14
x^2-y^2(+) 15a$_1$	−13.484	90	1	0	0	0	0	0	0	2
xz(−) 12b$_1$	−13.708	2	41	0	0	1	4	0	0	49
yz(+) 8a$_2$	−14.183	0	0	52	0	0	0	0	0	44

^{a} Mn d orbitals are labeled using an abbreviated notation, e.g., xz standing for d$_{xz}$ (see Chart 1 for axes orientations). ^{b} Total contributions from N(NH$_3$) and O′(formate).

17a$_1$ and 15b$_1$), as anticipated on the basis of simple LF considerations (Figure 5).

From Table 2 two of the Mn d-based occupied spin-up MOs are calculated to have large contributions from μ-oxo p orbitals, i.e., levels 12b$_2$ (yz(−) mixed with p$_{y'}$) and 16a$_1$ (xz(+) mixed with p$_{z'}$). Transitions from these orbitals are expected to be dominant in the absorption spectrum as they involve significant oxo → Mn charge transfer (CT) character. From level 12b$_2$ only the transition to 17a$_1$ is allowed in C_{2v} symmetry, yz(−) → z^2(+) for **E** || **y(a)**, while both 16a$_1$ → 17a$_1$ and 16a$_1$ → 15b$_1$ are allowed in **E** ⊥ **y(a)** polarization. Thus, a single intense band is expected for **E** || **y(a)**, as observed (Figure 3), supporting the assignment of band *II* to ^{9}A$_1$ → ^{9}B$_2$(yz). The two possible assignments for the **E** ⊥ **y(a)** polarized absorption band *III*, i.e., 16a$_1$ → 17a$_1$ or 15b$_1$, can be evaluated on the basis of the orbital compositions in Table 2. Calculations have shown that the dominant contribution to transition intensities involves a sum of overlaps of individual ligand orbitals contributing to the corresponding donor and acceptor MOs.[49] Since the donor orbital, 16a$_1$, has a high oxo p$_{z'}$ character, the intensity of transitions from this level will critically depend on the oxo p$_{z'}$ admixture to the acceptor orbital. Thus, band *III* is assigned to xz(+) → z^2(+) (^{9}A$_1$ → ^{9}A$_1$(xz) in Figure 5) since of the two z^2-based acceptor orbitals only 17a$_1$ has oxo p$_{z'}$ character. While the **E** ⊥ **y(a)** polarized transitions ^{9}A$_1$ → ^{9}A$_1$(x^2-y^2) and ^{9}B$_1$(x^2-y^2) (cf. Figure 5) are obscured by intense CT absorptions (Figure 3), an experimental lower limit of 23 000 cm^{-1} is obtained for their energies. From the position of band *II* (~13 500 cm^{-1}), this gives an energy splitting of the π antibonding t$_{2g}$ set of Mn d orbitals greater than 9500 cm^{-1}, providing a direct measure of the strong Mn(III)−O(oxo) π bonding interaction.

For comparison with the experimental data, the energies of the transitions from yz(−) and xz(+) to z^2(+) were calculated from the differences in total energy of the excited and ground states at convergence. The calculated energies of 12 970 and 19 520 cm^{-1} compare favorably to the experimental values of 13 500 and 20 500 cm^{-1} and justify a more detailed consideration of the calculated orbital descriptions. Boundary surface plots of the three orbitals involved in the two dominant LF absorptions of [Mn$_2$O(OAc)$_2$(Me$_3$tacn)$_2$](ClO$_4$)$_2$·H$_2$O (bands *II* and *III*) are shown in Figure 6. The (−) combination of Mn yz orbitals has a very strong π antibonding interaction with the

(49) (a) Ros, P.; Schuit, G. C. A. *Theor. Chim. Acta (Berlin)* **1966**, *4*, 1. (b) Van der Avoird, A.; Ros, P. *Theor. Chim. Acta (Berlin)* **1966**, *4*, 13.

Figure 6. Boundary surface plots of the Mn d-based occupied xz(+) and yz(−) and unoccupied z^2(+) spin-up MOs obtained from a spin-unrestricted HS calculation on μ-O Me$_3$tacn.

oxo p$_{y'}$ orbital. This leads to a large destabilization of the yz(−) MO and mixes CT character into the yz(−) → z^2(+) transition. Both the low energy and high intensity of band *II* (Figures 2−4) are thus a clear fingerprint for the presence of an oxo bridge in the [Mn^{III}$_2$O(OAc)$_2$L$_2$]$^{2+}$ complexes. Due to the bent Mn−O−Mn structure the π antibonding interaction between the manganese xz and oxo p$_{z'}$ orbitals is weaker, and the xz(+) → z^2(+) transition is thus at higher energy than yz(−) → z^2(+). The high intensity of this transition (band *III*), which is roughly an order of magnitude more intense than typically observed for octahedral Mn(III) complexes,[28] results from a large contribution of the oxo p$_{z'}$ orbital to both the donor and acceptor orbitals. Notice, however, that similarly intense d → d transitions are observed for five-coordinate Mn(III) complexes where the large deviations from inversion symmetry allow for stronger mixing between LF and CT excited states.

In summary, the oxo bridge in [Mn^{III}$_2$O(OAc)$_2$L$_2$]$^{2+}$ dimers produces a number of spectral features (Figures 2−4) that appear to be unique among octahedral Mn(III) complexes: (i) a prominent absorption and MCD band (*II*) at ~13 500 cm^{-1}, (ii) unusually high intensity of the characteristic Mn(III) absorption band (*III*) around 20 000 cm^{-1}, and (iii) an exceptionally large splitting of the t$_{2g}$ set of Mn d orbitals exceeding 9500 cm^{-1}. The structural implications of these results for the active site of OxMnCAT are discussed below.

Structural Implications for OxMnCAT. Extensive model studies have shown that the position of the lowest-energy absorption band of Mn(III) complexes provides information about the coordination number.[26,27] For six-coordinate complexes it corresponds to the e$_g$ intraset transition and is usually observed between 5000 and 12 000 cm^{-1}, in accordance with the presence of band *I* at ~10 000 cm^{-1} in the spectra of the six-coordinate μ-oxo-bridged Mn(III) model complexes (Figures 2 and 4). The lack of a similar feature in the spectra of OxMnCAT (Figure 1) shows that the HOMO/LUMO splitting

for both Mn(III) ions of the active site is larger, i.e., ~14 500 cm^{-1} (band *A*, Figure 1 and Table 1). From comparison to model data[26,27] this indicates that the two metal centers are five-coordinate.[50] Thus, the high absorption intensity of OxMnCAT at ~21 000 cm^{-1} does not necessarily reflect the presence of an oxo bridge at the active site as this is also typical of five-coordinate Mn(III) complexes.

In the case of the $[Mn^{III}_2O(OAc)_2L_2]^{2+}$ model complexes the Mn d-based donor and acceptor orbitals involved in transitions *II* and *III* have little contribution from ligands other than the bridging oxide (Figure 6, Table 2). A change from six-coordinate, roughly octahedral configuration of Mn(III) to five-coordinate ligation while maintaining the oxo bridge is therefore not expected to significantly perturb the corresponding absorption and MCD features. Thus, the large differences in the spectra of OxMnCAT (Figure 1) and the synthetic models (Figures 2−4), in particular the lack of band *II* in the protein spectrum, suggest the absence of an oxo bridge at the active site of OxMnCAT. On the basis of the spectral similarities to MnSOD, the presence of a weaker bridging ligand in OxMnCAT such as μ-OH$^-$ appears to be more likely. This will be further explored in section 3.

(2) Ground State. Analysis of the magnetization behavior of OxMnCAT allows refinement of the five-coordinate geometry of Mn(III) proposed on the basis of the absorption and MCD spectra. Figure 7 compares the MCD saturation magnetization curves plotted as a function of $\beta H/2kT$ for OxMnCAT and $[Mn_2O(OAc)_2(Me_3tacn)_2](ClO_4)_2\cdot H_2O$ ($J = +9$ cm^{-1} [45]). Also shown are the Brillouin curves[51] for $S = 2$ and $S = 4$ spin ground states, scaled to fit the data at small $\beta H/2kT$. (A plot of the $S = 2$ and $S = 4$ curves scaled for best reproduction of the low-temperature/high-field data is shown in Figure S3, Supporting Information.) The data are well fit by the Brillouin curve for an $S = 4$ ground state, and not $S = 2$ as from a pair of uncoupled high-spin Mn(III) ions. This demonstrates that the two manganese ions of the binuclear active site in OxMn-CAT are either ferromagnetically or very weakly antiferromagnetically coupled, thereby eliminating possible core structures such as di-μ-oxo-Mn$^{III}_2$ ($J \approx -90$ cm^{-1} [52,53]) or di-μ-alkoxo-Mn$^{III}_2$ ($J \approx -20$ cm^{-1} [1]).

The nesting behavior of the saturation magnetization curves indicates the presence of thermally accessible excited spin states. This is reflected in the low-field MCD data presented in the insets of Figure 7. Below 5 K deviations from the Curie behavior are observed involving a decrease in magnetic moment with decreasing temperature. Thus, in both dimers the $M_S = \pm 4$ component of the exchange-coupled ground state represents a low-lying excited state which, given the small nesting behavior, must be close to the ground state. For $[Mn_2O(OAc)_2$-$(Me_3tacn)_2](ClO_4)_2\cdot H_2O$ this has been verified by SQUID measurements.[45,54,55]

To interpret the MCD saturation data of OxMnCAT, we first consider the ground state of an exchange-coupled binuclear
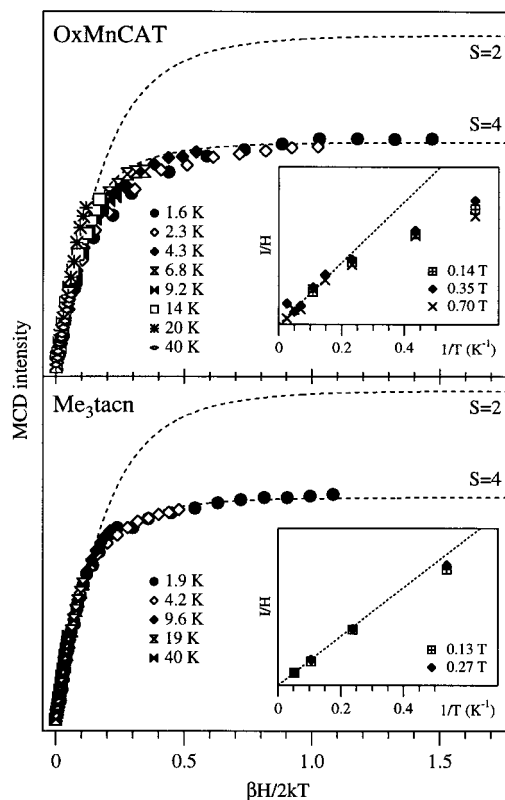
Figure 7. Saturation magnetization curves plotted as a function of $\beta H/2kT$ for OxMnCAT (recorded at 17 500 cm^{-1}) and $[Mn_2O(OAc)_2(Me_3$-tacn)$_2](ClO_4)_2\cdot H_2O$ (28 000 cm^{-1}). The $S = 2$ and $S = 4$ Brillouin curves scaled to fit the data at small $\beta H/2kT$ are shown by the broken lines. Insets: Low-field variable temperature MCD data and $1/T$ Curie function.

manganese(III) system. This can be approached using the following spin Hamiltonian:[56,57]

$$\mathcal{H} = -2J\mathbf{S}_1\cdot\mathbf{S}_2 + \sum_{i=1}^{2}\left\{D_i\left(\mathbf{S}_{zi}^2 - \frac{1}{3}S(S+1)\right) + E_i(\mathbf{S}_{xi}^2 - \mathbf{S}_{yi}^2) + g_i\beta\mathbf{H}\cdot\mathbf{S}_i\right\} \quad (1)$$

where J is the exchange coupling constant, D_i and E_i are the axial and rhombic zero-field splitting (ZFS) parameters of the two Mn ions ($i = 1, 2$), and $\mathbf{H}$ represents the magnetic field. Application of this Hamiltonian to an uncoupled basis set $|M_{S1}M_{S2}\rangle$ ($M_{Si} = 2, 1, ..., -2$) results in a 25×25 matrix which was diagonalized with $g_1 = g_2 = 2$ to obtain energies and wave functions of the dimer ground state.

First axial symmetry was assumed, i.e., $E_1 = E_2 = 0$, and the D values for the two Mn ions were set equal. Energy level diagrams for positive and negative D values, plotted as a function of $J/|D|$, are shown in Figure 8A. Two regions can be distinguished in each diagram corresponding to ferromagnetic ($J/|D| > 0$, $S = 4$ ground state) and antiferromagnetic coupling ($J/|D| < 0$, $S = 0$ ground state) between the two Mn ions.

(50) The possibility that the lowest-energy spin-allowed transition of OxMnCAT occurs beyond the experimentally accessible range (below 5000 cm^{-1}) can be eliminated for two reasons: (i) Jahn−Teller distortions in Mn(III) complexes will ensure a sufficiently large separation of the single unoccupied d orbital from the occupied orbitals and (ii) the low-lying excited state would spin−orbit couple to the ground state, giving rise to an imbalance between positive and negative MCD intensity.

(51) Kittel, C. *Introduction to Solid State Physics*, 6th ed.; Wiley & Sons: New York, 1986; pp 400−402.

(52) Kitajima, N.; Singh, U. P.; Amagai, H.; Osawa, M.; Moro-oka, Y. *J. Am. Chem. Soc.* **1991**, *113*, 7757.

(53) Glerup, J.; Goodson, P. A.; Hazell, R.; Hodgson, D. J.; McKenzie, C. J.; Michelsen, K.; Rychlewska, U.; Toftlund, H. *Inorg. Chem.* **1994**, *33*, 4105.

(54) Notice, however, that the large single-ion zero-field-splitting parameter of $D = +3$ cm^{-1} given in ref 45, obtained using a spin Hamiltonian that neglects rhombic distortions, appears to be incompatible with the small observed nesting behavior. Typical D values for μ-oxo-bridged Mn(III) dimers are ~0.3 cm^{-1}.[55]

(55) Vincent, J. B.; Tsai, H.-L.; Blackman, A. G.; Wang, S.; Boyd, P. D. W.; Folting, K.; Huffman, J. C.; Lobkovsky, E. B.; Hendrickson, D. N.; Christou, G. *J. Am. Chem. Soc.* **1993**, *115*, 12353.

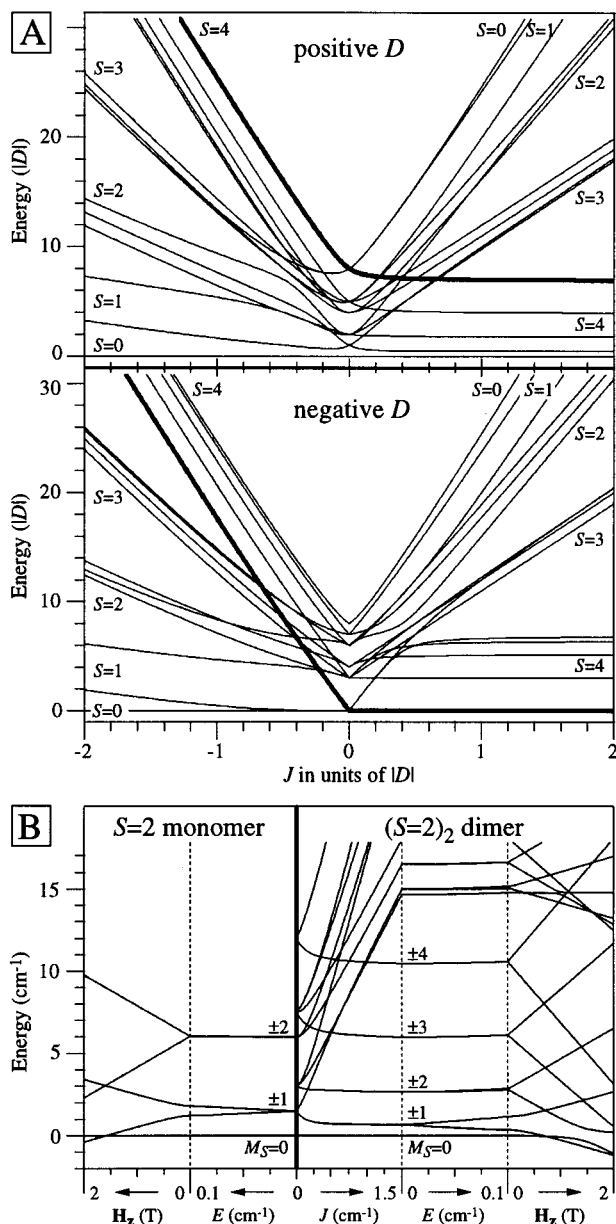(56) Kennedy, B. J.; Murray, K. S. *Inorg. Chem.* **1985**, *24*, 1552.

(57) Reem, R. C.; Solomon, E. I. *J. Am. Chem. Soc.* **1987**, *109*, 1216.

Figure 8. (A) Energy level diagrams for the ground state of an ($S = 2$)$_2$ dimer obtained from diagonalization of the spin Hamiltonian in eq 1 with $D_1 = D_2$ and $E_1 = E_2 = 0$. The $M_S = \pm 4$ component is highlighted by a thick line. (B) Effects of J, E and $\mathbf{H}_z$ on the ground state of an initially uncoupled Mn(III) dimer (right-hand side) and parallel data for a Mn(III) monomer (left-hand side), obtained with eq 1 and $D_1 = D_2 = 1.5$ cm^{-1}. The M_S components of the $S = 2$ monomer and $S = 4$ dimer ground states are indicated.

From the four possible sign combinations the one with positive J and negative D (right bottom portion of Figure 8A) can readily be excluded since in this case the $M_S = \pm 4$ component, highlighted by a thick line, constitutes the ground state of the dimer, and this is incompatible with the low-field MCD data (inset of Figure 7). The small nesting behavior of the saturation curves of OxMnCAT indicates that the separation of the $M_S = \pm 4$ component from the ground state is smaller than 20 cm^{-1}. From Figure 8A, for $J < 0$ cm^{-1} the energy of the $M_S = \pm 4$ component is roughly $20|J|$ if $D \leq 0$ cm^{-1} and higher if $D > 0$ cm^{-1}, placing a lower limit for J of ~ -1 cm^{-1}. Alternatively, the experimental data would be consistent with any value of $J > 0$ as long as D is also positive (top right portion in Figure 8A). Antiferromagnetic coupling between the two

Mn ions appears to be rather unlikey, although it cannot be excluded at this stage of the analysis.

Insight into the sign of J for OxMnCAT can be obtained from azide binding experiments (vide infra). Although azide binds to the active site, the saturation magnetization curves of the resting and azide bound forms of the protein are virtually identical[58] (Figure S3, Supporting Information). As exemplified by the series of μ-oxo-di-μ-carboxylato-bridged Mn(III) dimers, the nature of the terminal ligands has a significant effect on the sign and magnitude of J;[45,55] e.g., replacement of H_2O in [Mn$^{III}_2(\mu$-O)$(\mu$-O$_2$CR)$_2$(H$_2$O)$_2$(bpy)$_2]^{2+}$ by azide shifts the J value from -3.4 to $+8.8$ cm^{-1}. From Figure 8A a small change in J for $J/|D| < 0$ will strongly affect the energy of the $M_S = \pm 4$ component ($\Delta E(M_S = \pm 4) \approx 20\Delta J$) and, therefore, the saturation magnetization behavior. On the basis of the minor changes occurring upon azide binding to OxMnCAT it is concluded that J and D are most likely positive, in which case the splitting pattern of the $S = 4$ ground state is practically independent of the coupling constant, as observed[58] (right top portion of Figure 8A). Note that in principle the two Mn ions could have oppositely signed D values if their ligations were very different (positive and negative D values relate to holes in the z^2 and x^2-y^2 orbitals, respectively, vide infra). However, the monomer-like CD and MCD spectra of OxMnCAT reflect similar environments of the two metal ions, arguing against this possibility.

The last perturbations in the dimer ground-state analysis to be added are a rhombic distortion, expressed by the parameter E, and a magnetic field $\mathbf{H}$. Figure 8B (right-hand side) shows the ground-state splitting pattern for a stepwise inclusion of the different terms in eq 1. Starting with an uncoupled dimer composed of two monomers with D values of $+1.5$ cm^{-1}, which is in the range expected for OxMnCAT (vide infra) and MnSOD,[29] an increase in J from 0 to 1.5 cm^{-1} results in a fairly isolated $S = 4$ dimer ground state. As for the monomer, the dimer ZFS can be expressed in terms of an effective spin Hamiltonian, $\mathscr{H} = D'(\mathbf{S}_z^2 - (1/3)S(S + 1))$, where D' will be reduced relative to the monomer D, taking a value of $D' = (3/7)D$ in the strong exchange limit with $J \gg D$.[60] Inclusion of a rhombic ZFS component, $E = 0 \rightarrow 0.1$ cm^{-1}, only slightly affects the $M_S = \pm n$ levels with the exception of $M_S = \pm 1$. This is because the $\mathbf{S}_{xi}^2 - \mathbf{S}_{yi}^2$ term in eq 1 only mixes states with $\Delta M_S = \pm 2$ in first order, suggesting that the $M_S = \pm 2$, ± 3, and ± 4 levels can therefore be treated as pseudodoublets even in low symmetry. This is computationally verified by applying a magnetic field $\mathbf{H}$ along $\mathbf{z}$ (far right in Figure 8B), in which case the slopes of the spin sublevels relate to the magnetic moment. From these results it is concluded that the rhombic component of the ZFS splitting, E, only weakly perturbs the dimer ground state. In particular the $M_S = \pm 4$ component is essentially unaffected, suggesting that the saturation magnetization behavior of the dimer will be fairly independent of E.

(58) Using the formalism in ref 57 values for J and D can be estimated from a fit of the low-field MCD data. Although in the present case the large number of low-lying excited spin states (Figure 8) precludes an accurate determination of J and D, this provides a useful measure for a comparison between the resting and azide bound forms of the protein. Assuming identical transition intensities from each $M_S = \pm n$ level, good fits were obtained with $J > 0$ ($S = 4$ ground state) and D values of 0.38 cm^{-1} (resting enzyme) and 0.45 cm^{-1} (azide bound form). While the absolute D values have little meaning, their positive signs and similar magnitudes underline the high resemblance of the two data sets.

(59) Fee, J. A.; Shapiro, E. R.; Moss, T. H. *J. Biol. Chem.* **1976**, *251*, 6157.

(60) Bencini, A.; Gatteschi, D. *EPR of Exchange Coupled Systems;* Springer: Berlin, 1990; pp 48−57.

Chart 2. Transformation of μ-O Me$_3$tacn into Hypothetical Models for OxMnCAT and the Active Site Model for MnSOD
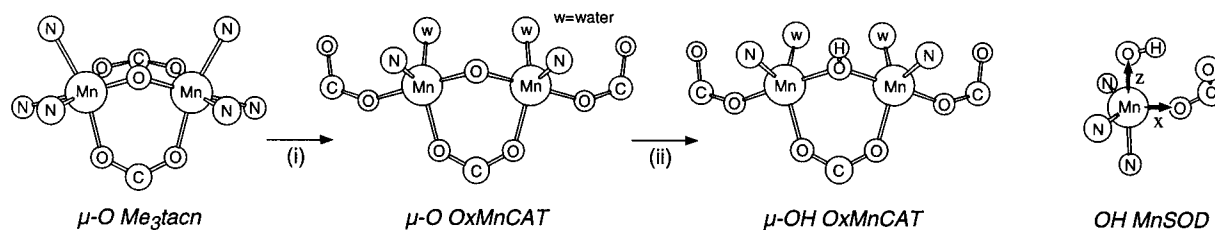
Two limiting geometries exist for a five-coordinate complex, trigonal bipyramidal and square pyramidal, which can be related by a Berry pseudorotation pathway maintaining C_{2v} symmetry.[29,61,62] For five-coordinate Mn(III) complexes the two possibilities can be distinguished from the sign of the ZFS parameter D. From second-order perturbation theory,[63] spin–orbit coupling among the LF states leads to a positive D in the trigonal bipyramidal limit (hole in the z^2 orbital) and a negative D in the square pyramidal extreme (hole in the x^2-y^2 orbital).[64] Thus, the positive sign of D derived from the saturation magnetization data of OxMnCAT reflects a trigonal bipyramidal limiting geometry for the two Mn(III) ions in the active site.[65] This is supported by the strong similarity of the MCD spectra of OxMnCAT and MnSOD[29] (Figure S1, Supporting Information), a crystallographically defined mononuclear enzyme with a five-coordinate, trigonal bipyramidal active site.[66] The saturation magnetization curves, however, exhibit stronger nesting in the case of MnSOD, initially suggesting that the ZFS of Mn(III) is larger in MnSOD than in OxMnCAT. Figure 8B (left-hand side) shows the ground-state splitting pattern for a Mn(III) monomer with $D = +1.5$ cm^{-1}, the value used for the dimer calculation. As discussed above the rhombic ZFS parameter E primarily quenches the magnetism of the $M_S \pm 1$ levels, and at low temperatures, i.e., low populations of the $M_S \pm 2$ pseudodoublet, the low-field MCD intensity will deviate significantly from the Curie behavior. In the monomer the $M_S \pm 2$ level is more than a factor of 2 higher in energy than in the dimer since $D > 2D'$. Thus, the stronger observed nesting for MnSOD than for OxMnCAT does not necessarily reflect a larger ZFS of Mn(III) in MnSOD.

In summary, the spectroscopic results of OxMnCAT, analyzed by reference to parallel data of μ-oxo-bridged binuclear Mn-(III) model complexes, lead to a model where the active site is comprised of two ferromagnetically coupled trigonal bipyramidal Mn(III) ions linked by a hydroxo bridge or an electronic structural analogue.

(3) Electronic Structure of OxMnCAT. Density Functional Calculations. In this section the experimental data presented above are used to evaluate density functional calculations on hypothetical models for OxMnCAT. Using the μ-O Me$_3$tacn model as a well-defined reference complex with respect to geometric and electronic structure (section 1), the correlation of geometric perturbations with changes in calculated electronic structure allows key structural features of the active site of OxMnCAT to be explored.

The above analysis, which indicates that the two Mn(III) ions of the active site in OxMnCAT are five-coordinate, is supported by preliminary crystallographic data on the enzyme isolated from *T. thermophilus*,[19] in which two five-coordinate manganese atoms are proposed to be linked by a Glu·CO$_2$ and two exogenous ligands (modeled as a water molecule and a μ-oxo atom in the oxidized form), and each metal is coordinated by a His·N and a monodentate Glu·CO$_2$. Thus, for the purposes of MO calculations, the first perturbation of the μ-O Me$_3$tacn geometry toward a model of the OxMnCAT active site involves removal of one NH$_3$ on each Mn atom, replacement of a bridging formate by two nonbridging water molecules, and replacement of the NH$_3$ groups trans to the oxo bridge by monodentate formates. This hypothetical model for the active site of OxMnCAT is shown in Chart 2 and will be referred to as μ-O OxMnCAT. The ligands around each manganese are arranged such that the bridging oxide and monodentate formate define the **z** axis and the three equatorial ligands complete a roughly trigonal bipyramidal coordination as required by the effective electronic symmetry (section 2).

Both high-spin (HS) and broken symmetry (BS) calculations were performed on this and the following models. Similar results were obtained using the two different computational schemes, and to facilitate comparison of the calculated electronic structures of hypothetical active site models, the following discussion is based on the results from BS calculations. In the BS formalism all the symmetry elements connecting the two metal ions in a dimer are removed, permitting the spin-up and spin-down densities to localize on opposite sides of the molecule.[67] Each spin-up orbital on one half of the dimer (Mn1) is energetically degenerate with a spin-down orbital on the other half (Mn2), and the spin-up and spin-down orbitals are mirror images of one another. Relevant parts of the energy level diagrams for the primarily Mn1-centerd MOs obtained from BS calculations on μ-O Me$_3$tacn and μ-O OxMnCAT are plotted relative to the energy of the respective LUMO in Figure 9 (left-hand side).[68] The four d electrons of Mn1 occupy spin-up orbitals, leading to a large stabilization by spin polarization of the Mn1 d-based spin-up MOs relative to their unoccupied spin-down counterparts and, therefore, to strong mixing with ligand orbitals. While this complicates direct analysis of the Mn1 d-based occupied spin-up MOs, a good description of these orbitals is provided by their unoccupied spin-down counterparts[69] (designated in Figure 9) as these reflect the uncompen-

(61) (a) Berry, R. S. *J. Chem. Phys.* **1960**, *32*, 933. (b) Berry, R. S. *Rev. Mod. Phys.* **1960**, *32*, 447.

(62) Rossi, A. R.; Hoffmann, R. *Inorg. Chem.* **1975**, *14*, 365.

(63) Ballhausen, C. J. *Molecular Electronic Structures of Transition Metal Complexes*; McGraw-Hill: London, 1979; pp 73−78.

(64) The sign change does not require that D passes through 0: Along the Berry pseudorotation coordinate, E increases to maximum rhombicity and a reorientation of the coordinate system is required.

(65) Note that this represents the effective electronic symmetry for the Mn ions and does not rule out distortion along a coordinate leading toward square pyramidal geometry.

(66) Ludwig, M. L.; Metzger, A. L.; Pattridge, K. A.; Stallings, W. C. *J. Mol. Biol.* **1991**, *219*, 335.

(67) Noodleman, L.; Norman, J. G., Jr. *J. Chem. Phys.* **1979**, *70*, 4903.

(68) All calculations performed on the OxMnCAT and MnSOD models afforded a monodentate carboxylate based HOMO mainly localized on the noncoordinating oxygen atom. In the protein this orbital will be stabilized by hydrogen bonding interactions, and it has therefore been omitted in the analysis of the computational results.

(69) Note that the Mn z^2-based unoccupied spin-down MO is stabilized relative to the other Mn d-based unoccupied spin down MOs (Figure 9) due to substantial delocalization onto Mn2 and/or mixing with the Mn 4s orbital.
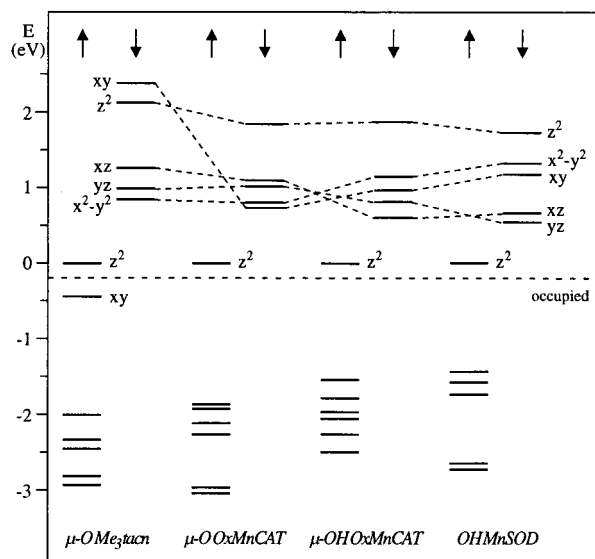
Figure 9. Relevant parts of the energy level diagrams obtained from BS calculations on the hypothetical model complexes in Chart 2, plotted relative to the respective Mn1-centered z^2-based spin-up LUMOs. For clarity, the occupied spin-down orbitals are not shown. Note that while the observed LF transitions are from the Mn d-based occupied spin-up orbitals, only their unoccupied spin-down counterparts are designated as these are less mixed with ligand orbitals.

sated spin-up density primarily localized on Mn1; see Table 3. (Note that the observed LF transitions are from the Mn d-based occupied spin-up orbitals to the single unoccupied, i.e., z^2, spin-up orbital.)

From Figure 9 transformation of μ-O Me$_3$tacn into μ-O OxMnCAT leads to a significant increase in the HOMO/LUMO gap, consistent with the lack of a near-IR transition in five-coordinate Mn(III) complexes and OxMnCAT. The Mn1 xy- and x^2-y^2-based unoccupied spin-down orbitals of μ-O OxMnCAT form a pair of moderately split MOs separated from a second pair at higher energy composed of the xz- and yz-based MOs. While this splitting pattern is typical of trigonal bipyramidal complexes, the energy order of the two pairs is reversed. This is due to a strong π antibonding interaction of the Mn xz and yz orbitals with the μ-oxo p orbitals (Table 3), paralleling the situation in μ-O Me$_3$tacn where the strong π antibonding interaction of the xz and yz orbitals has been experimentally verified (section 1). Thus, as anticipated on the basis of the dominant Mn$-$O(oxo) bonding interaction in the μ-oxo-bridged models, transformation of μ-O Me$_3$tacn into μ-O OxMnCAT only barely affects the xz-, yz-, and z^2-based MOs. The absorption spectrum of the hypothetical μ-O OxMnCAT model would thus be expected to be qualitatively similar to that of [Mn$_2$O(OAc)$_2$(Me$_3$tacn)$_2$](ClO$_4$)$_2$·H$_2$O in Figure 2 except for a large blue shift of band *I* ($xy \rightarrow z^2$) from ~10 000 cm^{-1} into the UV close to the x^2-$y^2 \rightarrow z^2$ transition. In this scenario bands A and B of OxMnCAT (Figure 1) would then have to correspond to bands *II* and *III* of the oxo-bridged Mn(III) dimers (Figures 2−4), which is inconsistent with their low absorption intensities relative to bands C and D (Table 1). Also the striking differences in the MCD spectra of OxMnCAT and the synthetic models (Figure 4) are difficult to rationalize given the dominant nature of the bridging oxide with respect to the electronic structure. Density functional calculations therefore support the experimental analysis that the presence of an oxo bridge at the active site of OxMnCAT is unlikely.

A second model for the active site was derived from μ-O OxMnCAT by protonation of the oxo bridge and readjusting

the bond lengths (μ-OH OxMnCAT in Chart 2). The relevant results obtained from a BS calculation on this structure are included in Figure 9 and Table 3. Protonation leads to a large stabilization of the oxygen p orbitals, in particular the p$_{z'}$ orbital as this is oriented toward the proton. The π antibonding interaction with the manganese d orbitals is therefore greatly reduced, evidenced by the low oxygen p contribution to the Mn d-based MOs (Table 3), and the Mn1 xz- and yz-based spin-down orbitals are displaced below the xy- and x^2-y^2-derived MOs (Figure 9). These results indicate that significant changes occur in the electronic structure upon protonation of the bridging oxide, suggesting that the key spectral features of the oxo-bridged Mn(III) dimers, shown in section 1 to derive from the strong Mn$-$O(oxo) π bonding interaction, will disappear. This was experimentally verified by measuring the absorption and MCD spectra of [Mn$_2$(OH)(O$_2$CC(CH$_3$)$_3$)$_2$(Me$_3$tacn)$_2$]$^{2+}$ (Figure S5, Supporting Information), a valence-localized μ-OH-bridged six-coordinate Mn(II)/Mn(III) mixed valence dimer.[70] Since all the Mn(II) LF transitions are spin forbidden, optical spectroscopy can be used to selectively study the Mn(III) monomeric half in this dimer. It was found that the absorption intensity below 25 000 cm^{-1} is significantly lower than in μ-oxo-bridged Mn(III) complexes, and, importantly, that band *II*, which is not observed for OxMnCAT (Figure 4), is also not present in the MCD spectrum of the μ-OH-bridged Mn(II)/Mn(III) dimer.

While mono-hydroxo-bridged five-coordinate Mn(III) dimers have not yet been isolated, a well-characterized reference complex for a comparison with μ-OH OxMnCAT is represented by MnSOD.[66] In the oxidized enzyme, Mn(III) is in a trigonal bipyramidal coordination with two His·N and a monodentate syn carboxylate oxygen in the equatorial plane and axial His·N and water or hydroxide ligands.[71,72] For the electronic structure calculations[73] this site was approximated by the OH MnSOD model in Chart 2, which is based on the crystallographic coordinates averaged for the two subunits.[66] The results from a spin-unrestricted calculation on OH MnSOD are included in Figure 9 and Table 3. Both the d orbital splittings and MO compositions are notably similar to the corresponding data for μ-OH OxMnCAT. In view of the high resemblance of the optical spectra of OxMnCAT and MnSOD[29] it appears that μ-OH OxMnCAT in Chart 2 is a reasonable active site model for OxMnCAT.

Ligand Field Calculations. To analyze in more detail the LF region in the absorption spectrum of OxMnCAT (Figure 1), angular overlap model (AOM)[74] calculations were performed on a monomeric unit of μ-OH OxMnCAT. The ligand positions expressed in terms of the two angles θ (rotation around the Mn$-$N(H$_3$) bond vector defined as the **y** axis) and ϕ (rotation around the Mn$-\mu$-O(H)) axis **z**) are given in Table 4. The AOM parameters e_σ and e_π for each ligand were fixed relative to an effective e_{eff} where the scaling factors (Table 4) are based on literature data[28,75] and account for the axial compression (unoccupied z^2 orbital). The Racah *B* parameter was set to 1000 cm^{-1}, and a *C/B* ratio of 4.0 was used (note that the quintet states all arise from the ^{5}D free-ion term; their energies are thus

(70) Bossek, U.; Hummel, H.; Weyhermüller, T.; Wieghardt, K.; Russell, S.; van der Wolf, L.; Kolb, U. *Angew. Chem., Int. Ed. Engl.* **1996**, *35*, 1552.

(71) To identify the nature of the solvent ligand, spin-unrestricted calculations were performed on both the water and hydroxide bound forms. A significantly better correspondence between the calculated and observed d orbital splittings was obtained for the hydroxide bound species, supporting recent proposals of an axial hydroxide ligand in oxidized MnSOD.[3,72]

(72) Fisher, C. L.; Chen, J.-L.; Li, J.; Bashford, D.; Noodleman, L. *J. Phys. Chem.* **1996**, *100*, 13498.

(73) Brunold, T. C.; Solomon, E. I. Unpublished results.

(74) Schäffer, C. E. *Struct. Bonding* **1968**, *5*, 68.

Table 3. Energies (eV) and Compositions (%) of the Unoccupied Spin-Down Counterparts of the Mn1 d-Based Occupied Spin-Up MOs Obtained from BS Calculations on the Models in Chart 2[a]

level	μ-O Me$_3$ tacn			μ-O OxMnCAT			μ-OH OxMnCAT			OH MnSOD		
	E_{rel}	Mn1	oxo	E_{rel}	Mn1	oxo	E_{rel}	Mn1	O(H)	E_{rel}	Mn	O(H)
xy	1.54	80	0	0.00	87	3	0.36	86	0	0.64	80	1
xz	0.40	61	17	0.36	58	14	0.00	69	2	0.12	84	3
yz	0.14	83	13	0.28	80	6	0.20	82	4	0.00	88	8
x^2-y^2	0.00	87	0	0.07	77	3	0.53	83	0	0.79	86	0

[a] Energies, E_{rel} (eV), are given relative to the spin-down LUMOs. Only Mn d and O(oxo) or O(hydroxo) p orbital contributions are given.

Table 4. Ligand Positions and Parameters Used for the Angular Overlap Model (AOM) LF Calculation on a Monomeric Unit of μ-OH OxMnCAT[a]

ligand	θ	ϕ	e_σ	e_π
μ-O(H)	0	0	1.00	0.15
O(CHO)	180	0	1.00	0.15
O(H$_2$)	90	205	0.90	0.10
N(H$_3$)	90	90	0.90	0.00
μ-O(CHO)	90	330	0.90	0.10

[a] Ligand positions are expressed in terms of the two angles θ (rotation around **y**) and ϕ (rotation around **z**). AOM parameters e_σ and e_π are in units of e_{eff} ($e_{eff} \approx 10\,250$ cm^{-1} for OxMnCAT).
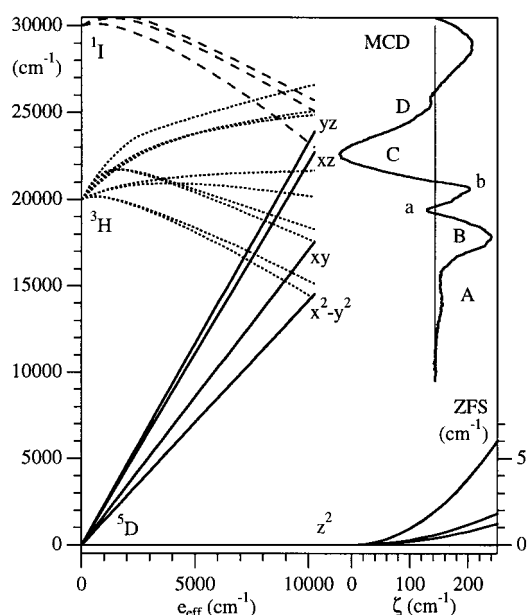
Figure 10. Relevant part of an energy level diagram from an AOM ligand field calculation on a monomeric unit of μ-OH OxMnCAT, obtained with the parameters in Table 4, and experimental 4.5 K MCD spectrum of OxMnCAT. The effect of spin−orbit coupling on the ground state is shown in the right bottom portion (note the scale change by a factor of 1000).

independent of B and C). An energy level diagram plotted as a function of e_{eff} is shown in Figure 10, along with the 4.5 K MCD spectrum of OxMnCAT. For $e_{eff} = 10\,250$ cm^{-1} the correspondence between the calculated and observed spectra is good. This permits an assignment of the spin-allowed transitions corresponding to bands A−D (cf. Table 1) and allows the sharp features a and b with little corresponding absorption and CD intensity (Figure 1) to be attributed to spin-forbidden transitions to the split ^{3}H term. Analogous calculations[73] on OH MnSOD produced an identical d orbital splitting pattern and afforded a similar value of $e_{eff} = 9870$ cm^{-1}, lending further support to the model that μ-OH OxMnCAT is a reasonable electronic structure description for the active site of OxMnCAT.

The effect of spin−orbit (SO) coupling on the ground state of a monomeric unit of μ-OH OxMnCAT is addressed in the

right bottom portion of Figure 10. SO coupling within the LF states lifts the 5-fold spin degeneracy of the ground state, producing a splitting pattern consistent with a positive ZFS parameter D. Using an effective spin Hamiltonian, $\mathcal{H} = D(S_z^2 - (1/3)S/S + 1)) + E(S_x^2 - S_y^2)$, the energies of the split components can be fit to determine D and E. Assuming that the spin−orbit coupling constant of Mn^{3+}, $\zeta_0 = 355$ cm^{-1}, will be reduced by covalency[76] to $\sim$70% in OxMnCAT, values of $D = 1.5$ cm^{-1} and $E = 0.1$ cm^{-1} are obtained. From Figure 8, in a ferromagnetically coupled dimer with $D_1 = D_2 = 1.5$ cm^{-1} the energy separation of the $M_S = \pm 4$ component from the $M_S = 0$ ground state is $\sim$10 cm^{-1}, consistent with the saturation magnetization data of OxMnCAT discussed in section 2.

(4) Azide Binding. Optical spectroscopy of OxMnCAT can be used to study the interaction of the active site with small anions which serve as mimics of hydrogen peroxide, thereby providing insight into the catalytic reaction mechanism. Given the similar electronic structures of azide and peroxide,[77] the reaction of Mn catalase with azide is of particular interest. Addition of azide to resting OxMnCAT (AzMnCAT) gives rise to an intense new feature at about 27 000 cm^{-1} in the low-temperature absorption and MCD spectra as shown in Figure 11 (arrows). While in absorption the LF region below 25 000 cm^{-1} is only slightly perturbed, MCD spectroscopy reveals a shift to lower energy of all the quintet LF excited states of Mn-(III) (bands A−D in Figure 1). These shifts were estimated from a Gaussian resolution of the MCD spectrum (Figure S4, Supporting Information) and are given in Table 1.[78] In contrast to the spin-allowed transitions there is a good correspondence between the two sets of spectra with respect to the positions of the sharper features attributed to spin−flip transitions. An absorption spectrum of AzMnCAT collected at 300 K is nearly superimposable on the one in Figure 11, indicating that the active site structure is not affected by the temperature.

The large differences in the optical spectra of OxMnCAT and AzMnCAT indicate that azide significantly perturbs the active site. Due to its high absorption intensity the new feature at 27 000 cm^{-1} is assigned as an azide → Mn CT transition. This indicates that azide binds directly to the Mn ions and appears to be the first direct evidence for azide binding to the active site of OxMnCAT. From the uniform shift of the spin-allowed LF transitions (bands A−D in Table 1) it is concluded that both Mn ions of the active site are similarly perturbed upon azide binding. The comparable intensities of the LF transitions below 25 000 cm^{-1} in the absorption spectra of the resting and azide bound enzymes strongly suggest that the coordination number of manganese does not increase upon azide binding as

(75) Lever, A. P. B. *Coord. Chem. Rev.* **1982**, *43*, 63.

(76) Gerritsen, H. J.; Sabisky, E. S. *Phys. Rev.* **1963**, *132*, 1507.

(77) Pate, J. E.; Ross, P. K.; Thamann, T. J.; Reed, C. A.; Karlin, K. D.; Sorrell, T. N.; Solomon, E. I. *J. Am. Chem. Soc.* **1989**, *111*, 5198.

(78) The quality of the fit (obtained under the assumption that the bandwidths do not change upon azide binding) suffers from large band distortions arising from spin−orbit coupling between the quintet and triplet LF excited states.
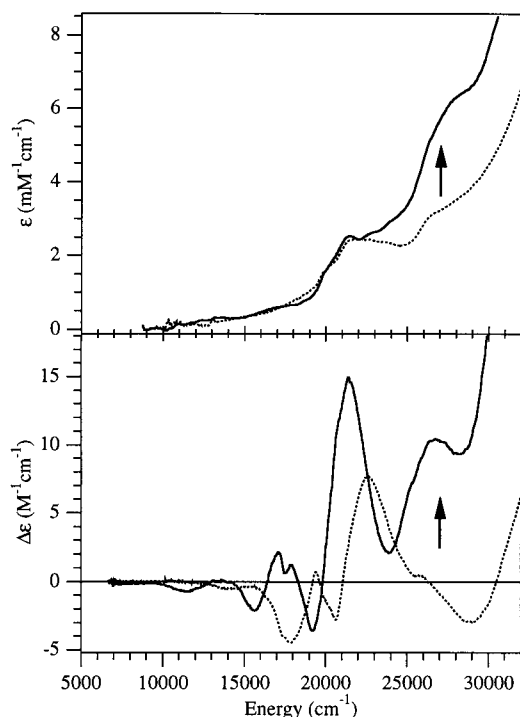
Figure 11. 15 K absorption and 4.5 K MCD (6 T) spectra of azide-perturbed Mn catalase (AzMnCAT), solid lines. For comparison, the spectra of resting OxMnCAT are reproduced from Figure 1, dotted lines.

this would lead to a significant reduction in intensity.[79] This conclusion is supported by the similar positions of the spin−flip transitions in the two sets of spectra since an increase in coordination number would result in a reduction of the Racah B and C parameters and, therefore, a red shift of the sharp features. Thus, azide appears to bind to both Mn(III) ions of the active site by displacement of one of the ligands on each metal, thereby retaining five-coordination.

These restrictions allow for three possible binding modes of azide to the active site: (i) bridging μ-1,1, (ii) bridging cis μ-1,3, and (iii) nonbridging end-on (one azide molecule per Mn). The highest energy fully occupied MOs of azide are an initially doubly degenerate set of π nonbonding orbitals,[77] π^{nb}. Upon binding to manganese, one π^{nb} orbital, π_σ^{nb}, forms a σ bond to Mn and is more strongly stabilized than the other π^{nb} orbital, π_v^{nb}, which is oriented perpendicular to the Mn−azide plane and thus involved in a weaker π bonding interaction. From Table 1 band A exhibits the largest red shift upon azide binding to OxMnCAT, indicating that the σ bonding interaction with azide mainly involves the Mn x^2-y^2 orbital. The fact that bands B and C, and thus the xy and xz orbitals, are similarly perturbed and to a greater extent than yz suggests that the π bonding interaction primarily involves these two orbitals. On the basis of these results, we favor a cis μ-1,3 bridging or a nonbridging end-on binding mode of azide to OxMnCAT, as in this case the x^2-y^2 orbital is most strongly destabilized and the positive ZFS parameter is retained,[80] consistent with our MCD results (section 2). Raman experiments are currently underway to evaluate the two possibilities.

Discussion

The manganese-containing catalases isolated from *T. thermophilus* and *L. plantarum* have been the subject of much recent work in bioinorganic chemistry.[5] Owing to the lack of an EPR signal and the facile X-ray photoreduction, however, very little is known about the Mn(III)/Mn(III) oxidation state of Mn catalase (OxMnCAT), and discussion of the reaction mechanism on a molecular level has necessarily been limited. In the following the key results obtained for the μ-oxo-bridged Mn-(III) model complexes and OxMnCAT are briefly summarized, and their significance with respect to the enzymatic peroxide disproportionation reaction are discussed.

Correlation of Spectral Features and Structural Elements. The similar overall protein folds of Mn catalase and hemerythrin, along with the fact that the absorption spectrum of OxMnCAT resembles those of μ-oxo-di-μ-carboxylato-bridged manganese-(III) dimers (Figures 1−3) have led to the idea that a $[Mn^{III}_2O(O_2CR)_2]^{2+}$ core may be present in OxMnCAT.[1,5,25] Five-coordinate Mn(III) complexes, however, are known to also exhibit an absorption spectrum very similar to that of OxMn-CAT.[26,29] A significantly better probe of the ligand field environment of Mn(III) is provided by MCD spectroscopy. While the MCD spectra of μ-oxo-di-μ-carboxylato-bridged Mn-(III) dimers are very similar to one another (Figure 4), indicating that the transitions below ∼30 000 cm^{-1} are inherent to the $[Mn^{III}_2O(O_2CR)_2]^{2+}$ core, they display striking differences from the protein spectrum, in particular a large imbalance between positive and negative intensity and the presence of two additional positive features in the near-IR (bands *I* and *II*).

Insight into the spectroscopy of μ-oxo-bridged Mn(III) model complexes is obtained from polarized single-crystal absorption data of $[Mn_2O(OAc)_2(Me_3tacn)_2](ClO_4)_2 \cdot H_2O$ (Figure 3), complemented by density functional electronic structure calculations. Band *I* at ∼10 000 cm^{-1} (Figures 2 and 4) corresponds to the e_g intraset transition; it is characteristic of octahedral Mn(III) complexes. The absorption intensity of band *III*, assigned to the $xz(+) \rightarrow z^2(+)$ transition ($^9A_1 \rightarrow {}^9A_1(xz)$ in Figure 5), however, is unusually high for six-coordinate Mn(III) complexes. This is due to a large contribution from the oxo p$_{z'}$ orbital to the Mn d-based donor and acceptor orbitals (Figure 6). Band *II* at ∼13 500 cm^{-1}, which is particularly prominent in the MCD spectrum (Figure 4), is assigned to the $yz(-) \rightarrow z^2(+)$ transition ($^9A_1 \rightarrow {}^9B_2(yz)$). The low energy of this feature relative to band *III* reflects a very strong π antibonding interaction between the antisymmetric combination of Mn yz orbitals and the oxo p$_{y'}$ orbital and the consequent destabilization of the corresponding MO ($yz(-)$, Figure 6). While five-coordinate Mn(III) complexes exhibit similarly high absorption intensity in the visible region, band *II* appears to be unique to μ-oxo-bridged Mn(III) dimers, thus providing a spectral probe for the presence of an oxo bridge in these dimers.

From comparison to model data,[26,27] the lack of any observable features below 12 000 cm^{-1} in the optical spectra of OxMnCAT (Figure 1) indicates that both Mn(III) ions of the active site are five-coordinate. This together with the positive ZFS parameter D derived from the saturation magnetization data suggests that the two Mn(III) ions have a trigonal bipyramidal effective electronic symmetry. Given the dominant nature of

(79) Addition of azide to MnSOD at 295 K results in a five-coordinate complex that interconverts to a six-coordinate species at low temperatures. This change in coordination number is accompanied by a decrease in integrated intensity of about 50%. Whittaker, M. M.; Whittaker, J. M. *Biochemistry* **1996**, *35*, 6762.

(80) An AOM LF calculation was performed for AzMnCAT using the parameters in Table 4 except for those of H$_2$O which were replaced by values appropriate of azide, i.e., $e_\sigma = e_{eff}$ and $e_\pi = 0.2e_{eff}$ relating to π_σ^{nb} and π_v^{nb}, respectively. The calculated shifts for bands A−C are ∼−600 cm^{-1} and for band D ∼+100 cm^{-1}. In view of the simplicity of this model the correspondence is satisfactory.
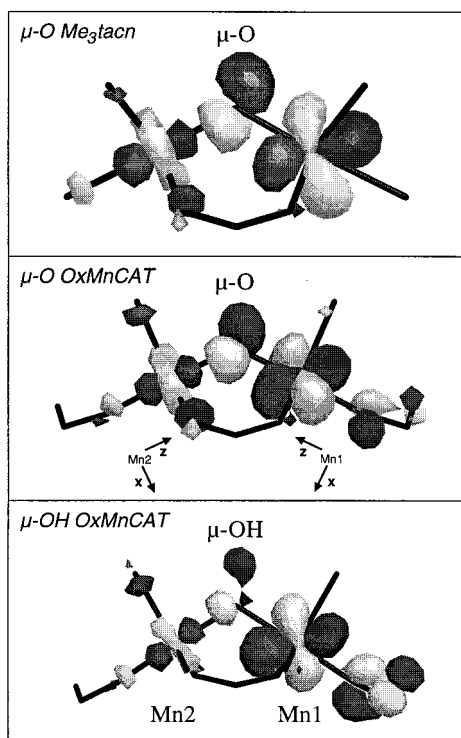
Figure 12. Boundary surface plots of the Mn1 *xz*-based unoccupied spin-down MOs obtained from BS calculations on the three dimers in Chart 2.
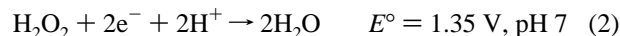
the bridging oxide with respect to the electronic structure of the μ-oxo-bridged Mn(III) complexes, the striking differences in the spectroscopy of OxMnCAT and the synthetic models (Figures 1−4), in particular the absence of band *II* in the protein spectra, make the presence of an oxo bridge at the active site unlikely. On the basis of the spectral similarities to MnSOD and supported by density functional electronic structure calculations, it is proposed that the Mn(III) ions of OxMnCAT are linked by a hydroxide bridge or an electronic structural analogue.

Effects of Protonation of the Oxo Bridge in μ-Oxo-Bridged Mn(III) Dimers. Boundary surface plots of the Mn1 *xz*-based unoccupied spin-down MOs obtained from BS calculations on the three dimers in Chart 2 are shown in Figure 12. The wave functions for the two μ-oxo-bridged dimers are practically identical, reflecting the dominant nature of the Mn−O(oxo) bonding interaction and its consequent weak dependence on changes in the remainder of the ligation (see also Table 3). Protonation of the oxo bridge greatly stabilizes the $p_{z'}$ orbital as this is involved in a σ bonding interaction with the proton. This virtually eliminates the bonding interaction of $p_{z'}$ with the Mn1 *xz* orbital (Figure 12). The lower negative charge on O(hydroxo) relative to O(oxo) also leads to a stabilization of the $p_{x'}$ and $p_{y'}$ orbitals and, consequently, to a smaller contribution of these orbitals to the Mn d-based MOs (Table 3). Overall, the Mn−O(hydroxo) bond is significantly weaker than the Mn−O(oxo) bond, and hydroxo-bridged Mn(III) dimers are expected to be considerably less stable than their oxo-bridged analogues. For Fe(III) dimers the weaker Fe−O(hydroxo) bond relative to Fe−O(oxo) is consistent with the longer Fe−O(H) bond length and the reduced exchange coupling.[81]

While synthetic hydroxo-bridged Mn(III) dimers have not yet been isolated, in iron chemistry the $(\mu\text{-OH})\text{−Fe}^{III}_2$ structural

unit is well-known in both proteins[4] (e.g., methane monooxygenase) and synthetic model complexes.[81,82] The pK_a in aqueous solution of oxo-bridged Fe(III) complexes lies in the range between 2.0 and 3.5, whereas similar Mn(III) dimers are prone toward rapid protonation even in neutral aqueous solution,[83] suggesting that their pK_a is higher. In OxMnCAT a hydroxo bridge will be further stabilized relative to an oxo bridge due to the hydrophobic environment[19] and the consequent reduction of the dielectric constant,[3] lending credence to the proposal of a hydroxo bridge at the active site. It might be anticipated that the orientation of the vacant Mn(III) z^2 orbital toward the bridging oxide would facilitate oxo → metal charge donation, initially suggesting that the pK_a values of these dimers might be lower relative to their Fe(III) analogues, in which the z^2 orbital is singly occupied. However, density functional calculations indicate that the negative charge on the bridging oxide is indeed higher in Mn(III) dimers than in analogous Fe(III) complexes[73] where spin polarization is sufficiently large to displace the occupied Fe d orbitals below the ligand valence orbitals, thereby enhancing oxo → Fe relative to oxo → Mn charge donation. Thus, the high pK_a values of oxo-bridged Mn-(III) dimers relative to their Fe(III) analogues appear well founded.

Mechanistic Implications. It has been shown that the disproportionation of peroxide by Mn catalase isolated from *L. plantarum* involves a ping-pong mechanism[22]

$$H_2O_2 + 2e^- + 2H^+ \rightarrow 2H_2O \qquad E° = 1.35\ V, \text{pH } 7 \quad (2)$$

$$H_2O_2 \rightarrow O_2 + 2e^- + 2H^+ \qquad E° = 0.28\ V, \text{pH } 7 \quad (3)$$

indicating that the two-electron redox potential must be fairly high, between 0.28 and 1.35 V.[84] In the heme catalases and peroxidases the peroxide reduction reaction (eq 2) is accomplished by an Fe(III)−protoporphyrin IX center that generates compound **I**, formulated as a ferryl porphyrin π-cation radical (O═Fe(IV)P•+).[85] This species catalyzes the peroxide oxidation reaction (eq 3) in catalases, or oxidizes substrates in the case of heme peroxidases. For horseradish peroxidase the one-electron reduction potential of the O═Fe(IV)P•+ species is $E° \approx 0.97$ V,[86] demonstrating that compound **I** is a very strong oxidant.

By analogy, it can be anticipated that the two-electron redox potential $E°$ of Mn catalase is also high and, therefore, that the reduced site is stabilized relative to OxMnCAT. This correlates well with the fact that the enzyme isolated from *L. plantarum* is not completely oxidized to OxMnCAT in air; rather the reduced site is always predominant.[22,87] Further, the observation of facile X-ray photoreduction of OxMnCAT appears to indicate that the energy barrier for reduction of the Mn(III)/Mn(III) active site to the Mn(II)/Mn(III) mixed valence form is small,[22] paralleling the observations for methane monooxygenase[88]

(82) Wu, F.-J.; Kurtz, D. M.; Hagen, K. S.; Nyman, P. D.; Debrunner, P. G.; Vankai, V. A. *Inorg. Chem.* **1990**, *29*, 5174.

(83) Wieghardt, K.; Bossek, U.; Nuber, B.; Weiss, J.; Bonvoisin, J.; Corbella, M.; Vitols, S. E.; Girerd, J. J. *J. Am. Chem. Soc.* **1988**, *110*, 7398.

(84) Sawyer, D. T. *Oxygen Chemistry;* Oxford University Press: New York, 1991; p 21.

(85) Xie, L. Y.; Dolphin, D. In *Handbook of Metal−Ligand Interactions in Biological Fluids;* Berthon, G., Ed.; Marcel Dekker: New York, 1995; pp 339−351.

(86) Hayashi, Y.; Yamazaki, I. *J. Biol. Chem.* **1979**, *254*, 9101.

(87) It is noteworthy that Mn catalase isolated from *T. thermophilus* undergoes complete autoxidation to the Mn(III)/Mn(III) level and that pH influences the rate but not the extent of oxidation. Khangulov, S. V.; Barynin, V. V.; Antonyuk-Barynina, S. V. *Biochim. Biophys. Acta* **1990**, *1020*, 25.

(81) (a) Armstrong, W. H.; Lippard, S. J. *J. Am. Chem. Soc.* **1984**, *106*, 4632. (b) Turowski, P. N.; Armstrong, W. H.; Liu, S.; Brown, S. N.; Lippard, S. J. *Inorg. Chem.* **1994**, *33*, 636.

where a μ-hydroxo bridge at the Fe(III)/Fe(III) active site has also been identified.[4] Insight into the redox properties of Mn catalase can be obtained from electrochemical studies of synthetic dimanganese(III) model complexes. The one-electron reduction potential in acetonitrile solution of an in situ generated hydroxo-bridged Mn(III) dimer, $[Mn_2OH(OAc)_2(Me_3tacn)_2]^{2+}$, is $E° \approx +1.05$ V, roughly 1 V more positive than for the oxo-bridged analogue ($E° \approx 0.02$ V).[83,89] For comparison, a reduction potential in acetonitrile of $E° \approx +1.05$ V was measured for a functional model of Mn catalase possessing an alkoxo-bridged core structure.[90,91] From these results it appears that formation of a weak Mn–O(hydroxo) bond instead of a strong Mn–O(oxo) bond at the active site of OxMnCAT will greatly reduce the relative stability of the oxidized site and thus ensure the necessary driving force for the peroxide oxidation reaction (eq 3).

In addition to the reduction potential, a second functionally significant property of Mn catalase is the rate of two-electron transfer from and to the substrate H_2O_2 molecule. A high rate requires a small reorganization to occur upon reduction/oxidation of the site and a large electronic coupling matrix element between H_2O_2 and the Mn(III) ions.[3] From our MCD studies, azide appears to bind to both Mn(III) ions of the active site by the displacement of one ligand on each metal, indicating that both manganese atoms are available for reaction with H_2O_2. Binding of peroxide in a cis μ-1,2 bridging mode, consistent with the spectroscopic data of AzMnCAT, would permit large electronic coupling to both Mn(III) ions and eliminate the need for an additional good superexchange pathway for two-electron oxidation of peroxide to dioxygen. Raman experiments are underway to evaluate possible azide binding modes.

To minimize the reorganization energy upon reduction, changes in the geometry of the active site of Mn catalase must be small. Since Mn(III) centers are potential Jahn–Teller systems, an important function of the protein is to impose an appropriate LF environment on manganese in the active site to eliminate any possible Jahn–Teller contribution to the reorganization energy. In Mn catalase this is achieved by a trigonal bipyramidal ligation of Mn(III), which gives rise to a large destabilization of the redox-active z^2 orbital relative to the other Mn d orbitals (cf. Figure 10). A second feature of Mn catalase that might assist in minimizing structural changes upon reduction is the proposed formation of a hydroxo bridge at the active site of OxMnCAT. Proton-coupled reduction of an oxo-bridged site would lead to a large change in geometry and, therefore, a large Franck–Condon barrier to substrate oxidation. This together with the high stability of the Mn–O(oxo) bond (low $E°$) could detrimentally affect the performance of Mn catalase by lowering the rate constant for the peroxide oxidation reaction.

The concepts discussed above are schematically illustrated by the potential energy diagrams in Figure 13, where oxy hemerythrin (oxyHr) has been chosen as a well-characterized example of a μ-oxo-bridged, hydrogen peroxide bound binuclear active site.[7] In the case of Mn catalase, coupling of the substrate oxidation reaction (eq 3) to reduction of OxMnCAT yields a
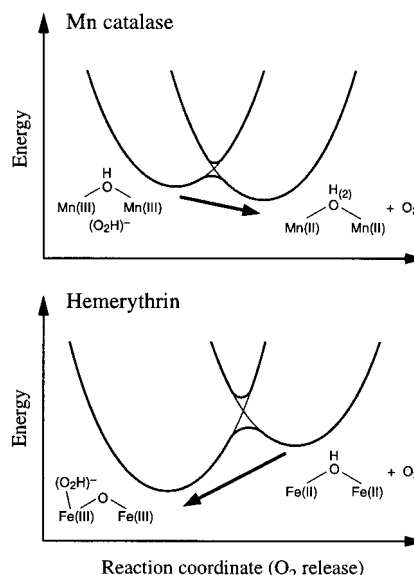
Figure 13. Schematic potential energy diagrams for the hydrogen peroxide oxidation reaction accomplished by OxMnCAT (top) and the dioxygen binding process of hemerythrin (bottom).

favorable overall process due to the anticipated high protein redox potential. While protonation of the hydroxo bridge will presumably occur upon reduction,[5] affording an aqua bridge at the reduced site, structural changes and thus the Franck–Condon barrier will be small (little displacement of the potentials along the reaction coordinate). These factors will make important contributions to the notably high rate of peroxide disproportionation by Mn catalase[21] ($k_{cat} = 2.0 \times 10^5$ s^{-1}). In hemerythrin the very strong Fe–O(oxo) bond stabilizes the diferric site relative to the reduced, hydroxo-bridged diferrous site. This yields a low reduction potential of oxyHr[92] and permits coupling of the two-electron reduction of dioxygen, the reverse reaction of eq 3, to oxidation of the diferrous active site. From crystallography,[7] deprotonation of the bridging hydroxide upon dioxygen binding to hemerythrin leads to a substantial Fe–O bond length decrease by $\sim$0.2 Å, indicated by a large displacement of the potentials in Figure 13. Overall, the oxo bridge in oxyHr makes a dominant contribution to both the formation and stabilization of the hydrogen peroxide bound species; the O_2 binding and dissociation constants are $k_{on} \approx 1 \times 10^7$ M^{-1} s^{-1} and $k_{off} \approx 50$ s^{-1}, respectively.[7] While the high stability of the peroxide bound oxy form is crucial for proper functioning of the dioxygen carrier protein hemerythrin, it would be fatal for catalases.

The importance of protein control of the protonation state at the active site with respect to catalytic activity is not unique to MnCAT. In contrast to oxyHr, the diferric peroxide intermediates of methane monooxygenase (MMO) and ribonucleotide reductase (RR) lack an oxo bridge at their active sites. These sites are therefore unstable toward formation of an Fe–O(oxo) bond in high-valent intermediates,[3] designated **Q** (MMO) and **X** (RR), that are essential for catalysis.[4] In the case of the oxygen-evolving complex (OEC) of photosystem II, the manganese cluster traverses five oxidation states during catalysis.[93] The energetics of the OEC leave little margin for inefficiency in the electron transfers upon each of the intermediate Kok state advancements, and the successive electron transfers must be

(88) Ericson, A.; Hedman, B.; Hodgson, K. O.; Green, J.; Dalton, H.; Bentsen, J. G.; Beer, R. H.; Lippard, S. J. *J. Am. Chem. Soc.* **1988**, *110*, 2330.

(89) Originally reported vs Fc$^+$/Fc, +0.55 V correction factor. Que, L., Jr.; True, A. E. In *Progress in Inorganic Chemistry: Bioinorganic Chemistry;* Lippard, S. J., Ed.; Wiley: New York, 1990; p 181.

(90) For this species the Mn$_2$(II/II)/Mn$_2$(II/III) and Mn$_2$(II/III)/Mn$_2$(III/III) reduction potentials are identical.

(91) (a) Pessiki, P. J.; Khangulov, S. V.; Ho, D. M.; Dismukes, G. C. *J. Am. Chem. Soc.* **1994**, *116*, 891. (b) Pessiki, P. J.; Dismukes, G. C. *J. Am. Chem. Soc.* **1994**, *116*, 898.

(92) The proton-coupled one-electron reduction potential of methemerythrin is $E° = +110$ mV. Armstrong, F. A.; Harrington, P. C.; Wilkins, R. G. *J. Inorg. Biochem.* **1983**, *18*, 83.

(93) Baldwin, M. J.; Pecoraro, V. L. *J. Am. Chem. Soc.* **1996**, *118*, 11325.

accomplished without the potential of the OEC becoming so high that early, incomplete oxidation of water occurs. On the basis of model data it was proposed[93] that these electrochemical requirements may be satisfied by coupling of proton transfer to electron transfer, which, similar to the situation in MnCAT, would allow the OEC to control the energy for each change in oxidation state.

In summary, analysis of the spectroscopic data of OxMnCAT leads to the proposal that the active site consists of two ferromagnetically coupled five-coordinate Mn(III) ions linked by a hydroxo bridge. The formation of a hydroxo bridge instead of an oxo bridge results in a high reduction potential of OxMnCAT and a small Franck−Condon barrier to electron transfer, both essential requirements for efficient catalytic turnover.

Supporting Information Available: Comparison of MCD spectra of OxMnCAT and MnSOD, energy level diagram from HS calculation on μ-O Me$_3$tacn, comparison of saturation magnetization curves for OxMnCAT and AzMnCAT, Gaussian fit of the MCD spectrum of AzMnCAT, 4.5 K absorption and MCD spectra of the μ-OH Mn(II)/Mn(III) dimer, and input coordinates for density functional calculations (9 pages, print/PDF). See any current masthead page for ordering information and Web access instructions.

JA981394L